Ore Geology Reviews 117 (2020) 103297

Contents lists available at ScienceDirect

Ore Geology Reviews

journal homepage: www.elsevier.com/locate/oregeorev

Geochronology, geochemistry and Hf isotopic composition of Late Cretaceous Laojunshan granites in the western Cathaysia block of South China and their metallogenic and tectonic implications

Guang-shu Yang[a], Han-jie Wen[b], Tao Ren[a,*], Sai-hua Xu[a], Cai-yan Wang[a]

[a] Faculty of Land Resources Engineering, Kunming University of Science and Technology, Kunming 650093, PR China
[b] Institute of Geochemistry, Chinese Academy of Sciences, Guiyang 550081, PR China

ARTICLE INFO

Keywords:
Zircon U–Pb age
Geochemistry
Hf isotope
Sn–W–In mineralization
Western Cathaysia block

ABSTRACT

Sn-, In- and W-rich granites are identified in Laojunshan area in the western Cathaysia block, South China, including coarse-grained two-mica monzogranite (CMG) and fine-grained two-mica monzogranite (FMG). Laser ablation-inductively coupled plasma-mass spectrometry (LA-ICP-MS) zircon U–Pb dating of CMG and FMG are from 85.6 ± 0.8 Ma to 90.37 ± 0.7 Ma and 89.9 ± 1.4 Ma, respectively. All samples have relatively high total alkalis contents (5.74 wt% to 9.73 wt%) and Al saturation indices (0.95 to 1.79), indicating that most of granites belong to the strongly peraluminous granites. The granites are enriched in P, Rb, Cs, Sn, Li, Be, and U, and are depleted in Ti, Mg, Co, Ni, Sr, Ba, Zr, and Hf. The fractional crystallization of plagioclase and K-feldspar was the principal process of magmatic differentiation that controlled Rb, Sr, Ba and Eu concentrations. While rare earth elements were fractionated by accessory minerals such as apatite, monazite or ilmenite. These geochemical features suggest that most of rocks are highly fractionated S-type granites. The εHf(t) values of the zircon samples from CMG and FMG range from −12.88 to −1.19, with the two-stage Hf model ages ranging from 1.2 Ga to 1.9 Ga. The geochemical and isotopic data show that the Laojunshan granites are derived from a crystalline basement that has metamorphosed pelitic rocks from the Mes-paleoproterozoic continental crust. The upwelling of the asthenosphere caused by a strong lithospheric extension led to the partial melting of the metamorphosed pelitic rocks to form widespread Late Cretaceous S-type granites in the Laojunshan area. Lithospheric extension and Cretaceous magma in SE Yunnan are probably related to the Palaeo-tethys ocean crustal delamination, which subducted beneath the Indochina block.

1. Introduction

Spatially and temporally, tungsten–tin (± indium) mineralization is generally associated with intrusive granite rocks (Hua et al., 2007, 2010; Mao et al., 2007, 2008; Xu et al., 2015). Previous studies have shown that large-scale W–Sn (± In) mineralization in South China is usually closely tied to Mesozoic granitic intrusions in mine (Hua et al., 2007, 2010; Liu et al., 2007; Mao et al., 2007, 2008; Cheng et al., 2009,2010a,2013,Cheng and Mao, 2010; Feng et al., 2010). Two-mica granites from Khuntan Batholith in Thailand (Yokart et al., 2003), fractionating Mole granites in Australia (Audétat et al., 2000), Cornwall granites in the U.K. (Müller et al., 2006), and Erzgebire granites in Germany (Breiter, 2012) have formed giant W–Sn deposits. Consequently, different types of granites associated with W–Sn mineralization had been named as “W–Sn bearing/rich granites” (Hua et al., 2007, 2010; Mao et al., 2007, 2008).

The SE Yunnan of China is located in the western Cathaysia block (Fig. 1a). Exposed in the region are three giant Cretaceous granite bodies, Gejiu, Bozhushan and Laojunshan, which are oriented equidistantly from one another along a NW direction (Fig. 1b). These granites are, respectively, related to the Gejiu world-class Sn–Cu–In polymetallic deposit, Bainiuchang super-large Ag–Sn–In polymetallic deposit, and Dulong world-class Sn–In polymetallic deposit (Zeng et al., 1998; Mao et al., 2008; Cheng et al., 2010a, Cheng and Mao, 2010). The Gejiu deposit has an estimated 0.38 Mt (million tons) of Sn reserves with an average grade of ~1%, an estimated 2500 t of In reserves, and Cu, Pb, Zn, Sb, Mo, and Bi reserves of over 1 Mt (Table 1; Zhang et al., 2003a,2003b; Cheng and Mao, 2010; Cheng et al., 2013). The Dulong Sn–In polymetallic deposit has explored Sn reserves of over 0.33 Mt with an average grade of 0.56%, Zn reserves of over 3.05 Mt with an average grade of 5.12%, about 5124 t of In reserves and is additionally enriched in Cu, Cd, Pb and Ga (Table 1; Zhang et al., 2003a,2003b; Ye

* Corresponding author.
E-mail address: rtao1982@126.com (T. Ren).

https://doi.org/10.1016/j.oregeorev.2019.103297
Received 25 February 2019; Received in revised form 18 December 2019; Accepted 20 December 2019
Available online 23 December 2019

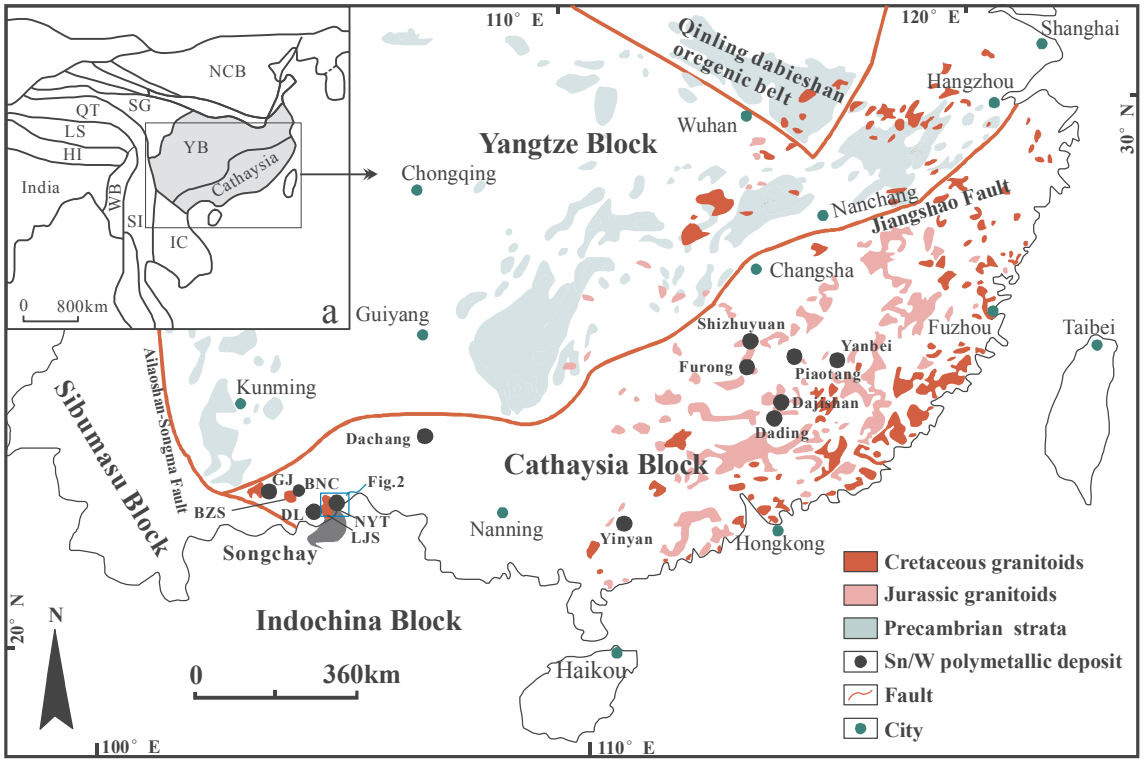

Fig. 1. (a) Simplified geological map of eastern Eurasia, showing major tectonic units (Wang et al., 2005). (b) Geological map showing the distribution of Jurassic and Cretaceous granites and representative Sn–W polymetallic deposits in the Cathaysia block, South China (modified by Cheng and Mao, 2010; Deng et al., 2012). The shape of Songchay is from Roger et al. (2000). NCB = North China block; YB = Yangtze block; IC = Indochina block; SI = Sibumasu block; SG = Songpan–Ganze; WB = West Burma; Hi = Himalayas; LS = Lhasa; QT = Qiangtang; GJ = Gejiu giant granite and world class Sn–Cu–In polymetallic deposit; BNC = Bainiuchang super large Ag–Sn–In polymetallic deposit; BZS = Bozhushan giant granite; LJS = Laojunshan giant granite; DL = Dulong world class Sn–In polymetallic deposit.

et al., 2016; Werner et al., 2017). Besides the Dulong Sn–In polymetallic deposit, several deposits have been found within the periphery of the Laojunshan granites, such as the Nanyangtian super-large W–B polymetallic deposit, Huangtian large-scale tungsten deposit, Xinzhai large-scale tin deposit, Saxi large-scale W–Li–Be deposit, the small-scale Changtian Pb–Zn deposit, and the Maka and Daping tungsten deposits (Table 1; Fig. 2; Li et al., 2013a). Therefore, SE Yunnan has become a world-class Sn–W–In–Cu–Pb–Zn polymetallic ore concentrated district (Figs. 1 and 2; Zeng et al., 1998; Mao et al., 2008; Ye et al., 2016).

The Laojunshan granites are exposed at the junction of Maguan County and Malipo County in SE Yunnan. The granite bodies are a compound rock mass with multiphasal magmatic emplacements and have a cambiform shape with a length of approximately 17 km from north to south, a width of 10 km from east to west, and an exposed area of about 153 km^2 (Fig. 2). Based on a review of regional geological survey reports, the granites appear to consist of three components, namely coarse-grained two-mica monzogranite, medium-fine-grained two-mica monzogranite, and porphyric granite (Fig. 2). In recent years, the geochemical characteristics of the granites have been determined and some high precision zircon U–Pb geochronological data have been obtained (Wang et al., 2014; Ye et al., 2016). However, samples that were used to indicate geochemical features of granite were not collected systematically and were mainly collected in the vicinity of the mining area where alteration by ore-forming fluids would likely occur. Furthermore, information on the geological setting of the granites are lacking and little is known about the relationship between the granites and the W–Sn–In polymetallic deposits in the region, even though they are located in the same area.

In this paper, core to rim samples were systematically collected near the village of Nanlao. The sample lithologies consisted mainly of coarse-grained two-mica monzogranite and fine-grained two-mica monzogranite. This paper report the results of laser ablation-inductively coupled plasma-mass spectrometry (LA-ICP-MS) zircon U–Pb dating, major element, trace element, and Hf isotopic data. The systematic geochemical data have provided useful information on the magma source, evolution, and the geological setting of the Laojunshan granites and an understanding of the W–Sn–In mineralization in the Laojunshan region.

2. Regional geology

The Laojunshan granites and related W–Sn–In polymetallic deposits are located in the western Cathaysia block, where the Yangtze block occurs to the north and the Indochina block to the south. The granites are located about 50 km from Wenshan city, Yunnan province. Tectonically, it lies within the Laojunshan metamorphic core complex (Figs. 1 and 2; LMCC). The LMCC is the northern part of the Song Chay Dome (Fig. 1b). At the core of the LMCC, the oldest metamorphic strata including Paleoproterozoic Nanyangtian formation (Pt_1n) and Saxi formation (Pt_1s), have been exposed through the effects of thrust nappe structures (Fig. 2; Bi et al., 2015). The Nanyangtian formation consists mainly of two-mica schist, plagioclasite-hornblende schist and carbonate (Bi et al., 2015). The Saxi formation consists of plagioclasite-hornblende schist, two-mica schist and carbonate (Bi et al., 2015). The Neoproterozoic Xinzhai formation (Pt_3x) presents in the western and northern parts of the study area (Fig. 2; Bi et al., 2015). It consists mainly of two-mica schist, biotite-quartz schist and marble (Fig. 2; Bi et al., 2015). Cambrian, Devonian, Carboniferous, Permian and Triassic strata consist of limestone, dolomite, sandstone, mudstone, phyllite and slate (Fig. 2; Bi et al., 2015).

Silurian gneissic granite crops out of the core of the LMCC (Fig. 2). Geochronological studies determined that the emplacement time of the

Table 1
Statistic intrusive ages of granites and mineralization ages of W–Sn deposits in SE Yunnan.

Deposit	Metal association	Deposit type	Reserves (t)	Ore minerals	Wall rocks	Related igneous rocks	Emplacement age	Mineralization age	References
Gejiu	Sn–Cu–In	Skarn vein	Sn 380,000 Cu 1,000,000 In 2500	Cassiterite, chalcopyrite, sphalerite, galena	Triassic, limestone, basalt	Gejiu granite batholith	77.4 ± 2.5 Ma to 85 ± 0.85 Ma	77.4 ± 0.6 Ma to 95.4 ± 0.7 Ma	Zhang et al., 2003a,2003b; Qin et al., 2006; Yang et al., 2008; Cheng et al., 2008, 2009,2013; Cheng and Mao, 2010; Cheng, 2012
Bainiuchang	Ag–Sn–In	Skarn vein	Sn 86,000 Ag 6470 Pb + Zn 2,820,000 In 1500	Cassiterite, chalcopyrite, sphalerite, galena	Cambrian, limestone, intrusive rock	Bozhushan granite batholith	86.51 ± 0.52 Ma to 91.6 ± 1.3 Ma	87.4 ± 3.7 Ma to 88.4 ± 4.3 Ma	Cheng et al., 2010b; Li et al., 2013c, d
Guanfang	W	Skarn	W 60,000	Scheelite, chalcopyrite	Cambrian, marble				Zhang et al., 2016
Dulong	Sn–In	Skarn	Sn 330,000 Zn + Pb 3,050,000 In 5124	Cassiterite, chalcopyrite, sphalerite, galena	Neoproterozoic Xinzhai Formation	Laojunshsn granite batholith	84.3 ± 2.2 Ma to 117.1 ± 0.9 Ma	75.04 ± 1.78 Ma to 93.6 ± 1.1 Ma	Lan et al., 2016; Liu et al., 2007, 2011, 2014; Li et al., 2013b; Wang et al., 2014; Ye et al., 2016; Wang et al., 2019
Nanyangtian	W–B	Skarn	W 340,000	Scheelite, tourmaline	Paleoproterozoic Nanyangtian Formation			97.49 ± 0.97 Ma and 118.14 ± 0.69 Ma,	
Xinzhai	Sn	Skarn Vein	Sn 50,000 Cu 10,000	Cassiterite, chalcopyrite, stibnite	Neoproterozoic Xinzhai Formation				
Saxi	W–Li–Be	Skarn	W 53,000	Scheelite, berylf	Paleoproterozoic Saxi Formation				
Changtian	Pb–Zn	Skarn	Zn + Pb 6500	Sphalerite, galena	Cambrian, phyllite, limestone				
Daping	W	Vein	W 5600	Scheelite, fluorite	Cambrian, phyllite, limestone				
Maka	W	Vein	W 6600	Scheelite, fluorite	Silurian, gneissose granite				

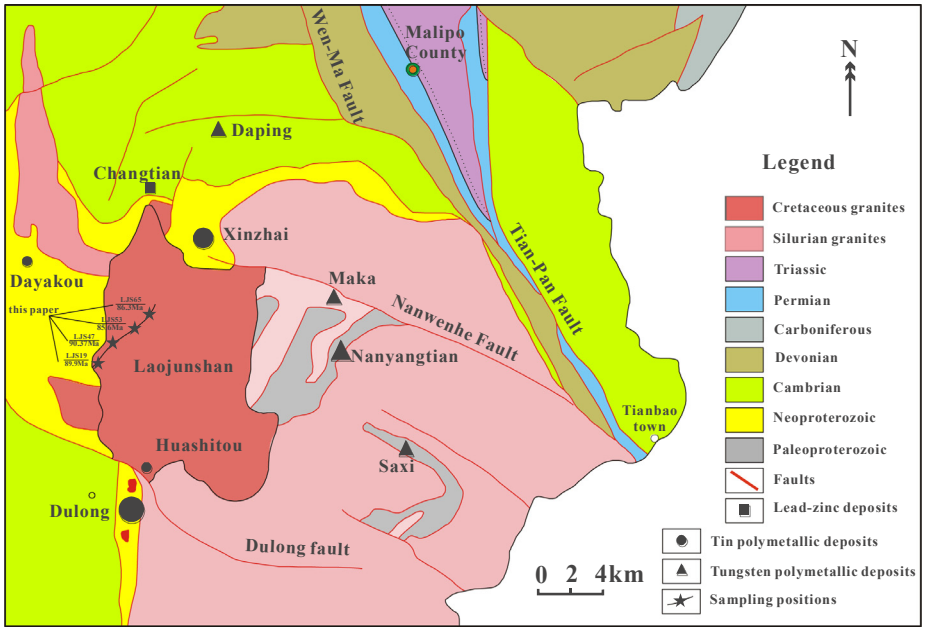

Fig. 2. Regional geological map of the Laojunshan area (modified by Bi et al., 2015).

gneissic granite was from ~390 Ma to ~430 Ma (Roger et al., 2000; Pan et al., 2015), and that the metamorphism time was primarily from 250 Ma Ma to 230 (Bi et al., 2015; Tan and Liu, 2017).

The NW trending sinistral strike-slip faults, which include the Wenshan-Malipo (Wen-Ma) fault, Maguan-Dulong fault (MDF) and Nanwenhe fault, the NNW trending Tianbao-Panjiapo (Tian-Pan) fault, which forms an arcuate line, and the Saxi and Nanyangtian thrusting-nappes are the ore-controlling faults in the region (Fig. 2; Bi et al., 2015). The NS trending Tongjie-Wukoudong and Yanshan-Nandangchang faults are secondary faults of the MDF. These faults control the Tongjie, Manjiazhai, Shuidongchang and Lazizhai ore blocks successively from north to south in the Dulong district. The Wen-Ma fault is related to the Huangtian tungsten deposit. The Nanyangtian and Saxi thrusting-nappe faults control the Nanyangtian and Saxi tungsten polymetallic deposits, respectively (Fig. 2; Bi et al., 2015). The Nanwenhe fault was involved in the formation of the Maka tungsten and Changtian Pb–Zn deposits (Fig. 2; Bi et al., 2015).

3. Sample preparation and analytical methods

3.1. Sample preparation

Granite samples were collected from the surface of the Nanlao village with the locations shown in Fig. 2. Thirty-six samples were collected for this study. These samples contain two different intrusion suits. (1) Coarse-grained two-mica monzogranite (CMG), which is pale gray in color with a coarse-grained granitic texture in the hand specimen (Fig. 3a). This granite consists of quartz (25% to 30%), plagioclase (20% to 25%), alkali feldspar (25% to 30%), biotite (6% to 8%), and muscovite (5% to 8%), as well as rutile, apatite, and zircon as accessory minerals (Fig. 3b, c). (2) Fine-grained two-mica monzogranite (FMG), which is gray to white in color with a fine-grained granitic texture in the hand specimen (Fig. 3d). This granite consists of quartz (25% to 30%), plagioclase (20% to 25%), alkali feldspar (20% to 25%), biotite (2% to 5%), and muscovite (10% to 15%), with rutile, apatite and zircon as accessory minerals (Fig. 3e, f).

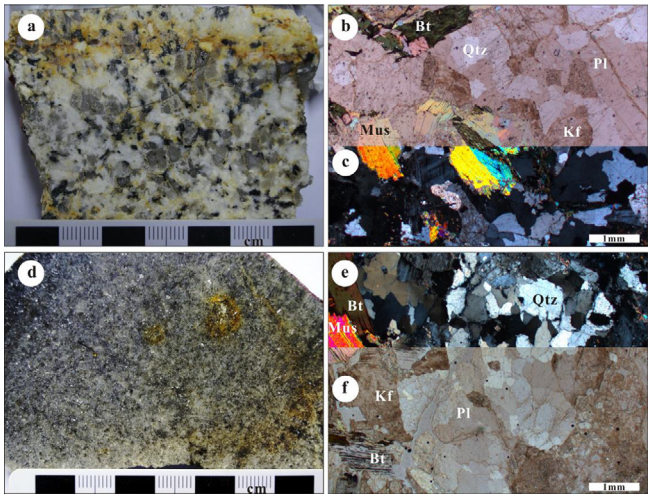

Fig. 3. Hand specimen photos of coarse-grained two-mica monzogranite (a, CMG) and fine-grained two-mica monzogranite in the Laojunshan district (d, FMG); photomicrographs of CMG (b) and FMG (f) under plane polarized light; photomicrographs of CMG (c) and FMG (e) under perpendicular polarized light. Bt = biotite; Qtz = quartz; Pl = plagioclase; Kf = potassium feldspar; Mus = muscovite.

3.2. Analytical methods

3.2.1. Major and trace element analyses

The analyses of major and trace elements were carried out at the State Key Laboratory of Ore Deposit Geochemistry (SKLODG), Institute of Geochemistry, Chinese Academy of Sciences. Whole-rock major element contents were determined by a PANalytical Axios X-ray fluorescence spectrometer on fused lithium tetraborate glass pellets with precisions better than 0.5%.

Trace elements were analyzed by a ELAN DRC-e ICP-MS. Powdered samples (50 mg) were dissolved with HF + HNO_3 in high-pressure Teflon bombs for 48 h at ~190 °C based on the method of Qi et al. (2000). Rh was used as an internal standard. The precision and accuracy of the data for the trace elements were determined using international standards GBPG-1, OU-6 and the Chinese National standard

GSR-1, and were generally better than 5%.

3.2.2. Zircon U–Pb dating and in situ zircon Hf isotope analysis

Zircon LA-ICP-MS U–Pb and Hf isotope analyses were carried out at the State Key Laboratory of Continental Dynamics, Xi'an, China. Individual zircon grains were separated from CMG and FMG samples using heavy liquid and magnetic separation methods, and then hand-picked under a binocular microscope. The zircon grains were fasten to an epoxy resin and polished to expose about half crystals for analyses. Cathodoluminescence (CL) images were collected using a CL spectrometer (Garton Mono CL3+) to identify the internal structure of the zircon grains. Zircon U–Pb isotopic dating was completed using a laser ablation-multiple collector-inductively coupled plasma-mass spectrometry (LA-MC-ICP-MS). Instruments include a Nu Plasma HR MC-ICP-MS (Nu Instruments Ltd., UK), an Elan6100 DRC Q-ICP-MS (Perkin Elmer/SCIEX, Canada) and a GeoLas 2005 excimer ArF laser-ablation system. The analytical methodology is described in detail by Yuan et al. (2008). Zircon 91,500 and NIST SRM610 were used as the external standard and used to optimize the results of the U–Pb dating respectively. Raw ICP-MS data were processed using software of GLITTER (Jackson, 2008) and ISOPLOT (Ludwig, 2003) to calculate the isotopic ages.

In situ zircon Lu–Hf isotope analyses were completed using LA-MC-ICP-MS. For the detailed instrumental parameters of the laser ablation system and MC-ICP-MS system see Yuan et al. (2008). The mass fractionation and interference corrected $^{176}Hf/^{177}Hf$ ratios were calibrated using the international standards 91,500 and Mud Tank. The initial $^{176}Hf/^{177}Hf$ values were calculated using the corresponding spot ages. Hf modal ages relative to depleted mantle were calculated using the assumed linear isotopic growth of depleted mantle from the $^{176}Hf/^{177}Hf$ ratios of 0.279718 at 4.55 Ga to 0.283250 at present, with a $^{176}Lu/^{177}Hf$ ratio of 0.0384 (Griffin et al., 2002).

4. Results

4.1. Zircon U–Pb geochronology

Four granite samples were selected for LA-ICP-MS zircon U–Pb dating. The weighted mean $^{206}Pb/^{238}U$ ages are quoted at the 95% confidence level. The zircon U–Pb concordia diagrams and all zircon CL images are shown in Fig. 4. Most of the zircon grains are euhedral with 100–300 μm long. The majority of zircon grains are transparent and colorless, and a few grains appear dark and opaque could induce by the high uranium content. The Pb, Th, and U contents are from 6.6 ppm to 94.8 ppm, from 45 ppm to 16792 ppm (Table 2), and from 275 ppm to 6386 ppm, respectively. The Th/U ratios of the samples range from 0.03 to 11.61 with a very strong positive correlation observed between Th and U, showing typical magmatic sources (Hoskin and Schaltegger, 2003; Hu et al., 2014). Few Th/U ratios are lower than 0.1, indicating that the sample crystallized in the later magma stage.

The analysis of zircon grains from samples LJS19, LJS47, LJS53 and LJS65 yield $^{206}Pb/^{238}U$ weighted mean ages of 89.9 ± 1.4 Ma (mean square weighted deviation, MSWD = 0.20), 90.37 ± 0.77 Ma (MSWD = 0.30), 85.6 ± 0.8 Ma (MSWD = 0.22) and 86.3 ± 0.46 Ma (MSWD = 0.47), respectively, and all of the points plot within or near the concordant curve (Fig. 4).

4.2. Major and trace elements

The results of major and trace elements analyses are summarized in Table 3. All of the samples are enriched in SiO_2 (SiO_2 = 69.1 wt% to 74.4 wt%). These rocks also have total alkalis (K_2O + Na_2O) contents of 5.74 wt% to 9.73 wt% and K_2O/Na_2O ratios are higher than 1 (from 1.07 to 25.8). On the alkalis vs. silica diagram, all of the samples fall within the granite field (Fig. 5a). The majority of rocks are strongly peraluminous (Fig. 5b), with A/CNK [= molar Al_2O_3/(CaO + Na_2O + K_2O)] ranging from 0.95 to 1.79.

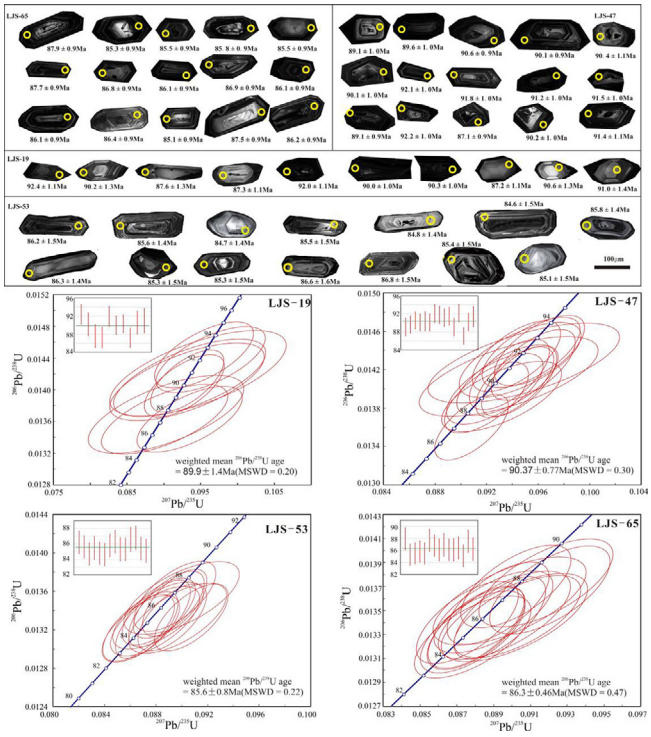

Fig. 4. Internal structure of zircon grains shown by the cathodoluminescence (CL) images and LA-ICP-MS zircon U–Pb Concordia age plots, weighted mean age plots for CMG and FMG.

The total rare earth element contents of the Laojunshan granites range from 8.48 ppm to 153.20 ppm. Chondrite-normalized REE patterns display a fractionated REE pattern (Fig. 6a). $(La/Yb)_N$ values range from 3.5 to 67.9 (Table 3), indicating a strong enrichment in light rare earth elements (LREEs). All of the samples have moderate Eu negative anomalies (Eu/Eu* = 0.18 to 0.70). In the trace element primitive mantle-normalized spider diagram (Fig. 6b), Laojunshan granites show enrichment of Rb, U, K, and Th, negative anomalies of Ba and Sr and significantly depleted of Nb, Ta and Ti. Selected major and trace elements are plotted against SiO_2 content in Fig. 7, showing a consistent linear trend.

4.3. Zircon Hf isotopic compositions

In situ zircon Hf isotopic results are shown in Table 4. The $^{176}Hf/^{177}Hf$ ratios vary from 0.282352 to 0.282686 (Fig. 8). εHf(t) values, calculated based on the $^{206}Pb/^{238}U$ age of the zircon grains, vary from −12.88 to −1.19 (Table 4; Fig. 8), with an average of −6.06. Two-stage Hf model ages (t_{DM2}) range from 1.9 Ga to 1.2 Ga (Table 4). In addition, the $f_{Lu/Hf}$ values of the zircon range from −0.93 to −0.99, which are much lower than those of the mafic crust (-0.34; Amelin et al. 2000) and sialic crust (-0.72; Vervoort et al. 1996). Therefore, the model ages can better reflect the time when the source material was extracted from the depleted mantle.

5. Discussions

5.1. Source and petrogenesis of the Laojunshan granites

The Laojunshan granites contain ~10% muscovite, and the whole-rock chemical compositions are enriched in SiO_2 (from 69.1 wt% to 74.4 wt%) and depleted in CaO (from 0.27 wt% to 0.92 wt%). K_2O/Na_2O ratios are from 1.07 to 25.8 and most of aluminum saturation indices (from 0.95 to 1.79) are higher than 1.1. Therefore, the majority

Table 2
LA-ICP-MS zircon U–Pb data for CMG and FMG from Laojunshan.

Sample	Elements (ppm)			Th/U	Isotopic ratios						ages (Ma)			
	Pb	Th	U		^{207}Pb /^{206}Pb	1σ	^{207}Pb /^{235}U	1σ	^{206}Pb/^{238}U	1σ	^{207}Pb/^{235}U	1σ	^{206}Pb/^{238}U	1σ
LJS19 (FMG)	25.3	779	1392	0.56	0.0479	0.0016	0.0954	0.0028	0.0144	0.0002	92.6	2.5	92.4	1.1
	16.3	180	1048	0.17	0.0479	0.0024	0.0931	0.0043	0.0141	0.0002	90.4	4.0	90.2	1.3
	79.7	16,792	1446	11.61	0.0478	0.0025	0.0902	0.0043	0.0137	0.0002	87.7	4.0	87.6	1.3
	24.8	376	1596	0.24	0.0479	0.0021	0.0901	0.0035	0.0136	0.0002	87.6	3.3	87.3	1.1
	25.2	45	1622	0.03	0.0486	0.0018	0.0964	0.0030	0.0144	0.0002	93.4	2.8	92.0	1.1
	26.6	844	1518	0.56	0.0479	0.0014	0.0928	0.0022	0.0141	0.0002	90.1	2.1	90.0	1.0
	78.8	3777	4113	0.92	0.0479	0.0014	0.0932	0.0020	0.0141	0.0002	90.4	1.9	90.3	1,0
	37.5	3632	1473	2.47	0.0498	0.0018	0.0935	0.0029	0.0136	0.0002	90.7	2.7	87.2	1.1
	11.8	225	703	0.32	0.0479	0.0024	0.0935	0.0042	0.0142	0.0002	90.7	3.9	90.6	1.3
	28.1	223	1782	0.13	0.0483	0.0027	0.0946	0.0049	0.0142	0.0002	91.8	4.6	91.0	1.4
LJS47 (CMG)	12.1	422	539	0.78	0.0485	0.0013	0.0932	0.0019	0.0139	0.0002	90.4	1.8	89.1	1.0
	29.2	601	1595	0.38	0.0480	0.0012	0.0926	0.0015	0.0140	0.0002	89.9	1.4	89.6	1.0
	57.0	316	3570	0.09	0.0480	0.0011	0.0938	0.0013	0.0142	0.0002	91.0	1.2	90.6	0.9
	40.7	385	2472	0.16	0.0487	0.0011	0.0945	0.0012	0.0141	0.0002	91.7	1.1	90.1	0.9
	14.9	204	828	0.25	0.0481	0.0017	0.0937	0.0028	0.0141	0.0002	90.9	2.6	90.4	1.1
	37.2	292	2263	0.13	0.0485	0.0011	0.0942	0.0012	0.0141	0.0002	91.4	1.2	90.1	0.9
	37.4	1122	1827	0.61	0.0481	0.0012	0.0955	0.0016	0.0144	0.0002	92.6	1.4	92.1	1.0
	20.7	357	1106	0.32	0.0477	0.0011	0.0943	0.0014	0.0143	0.0002	91.5	1.3	91.8	1.0
	68.2	416	4249	0.10	0.0487	0.0011	0.0956	0.0013	0.0143	0.0002	92.7	1.2	91.2	1.0
	35.2	1976	1201	1.64	0.0480	0.0013	0.0946	0.0019	0.0143	0.0002	91.8	1.8	91.5	1.0
	36.8	1141	1845	0.62	0.0479	0.0011	0.0920	0.0013	0.0139	0.0002	89.3	1.2	89.1	0.9
	35.5	544	1929	0.28	0.0484	0.0011	0.0961	0.0014	0.0144	0.0002	93.2	1.3	92.2	1.0
	58.1	192	3848	0.05	0.0484	0.0011	0.0908	0.0011	0.0136	0.0001	88.3	1.1	87.1	0.9
	78.4	5285	2409	2.19	0.0482	0.0012	0.0936	0.0016	0.0141	0.0002	90.9	1.5	90.2	1.0
	6.6	224	275	0.81	0.0482	0.0018	0.0949	0.0030	0.0143	0.0002	92.0	2.8	91.4	1.1
LJS53 (CMG)	52.4	4851	2193	2.21	0.0480	0.0016	0.0890	0.0018	0.0135	0.0002	86.6	1.7	86.2	1.5
	73.5	435	4959	0.09	0.0479	0.0015	0.0883	0.0016	0.0134	0.0002	85.9	1.5	85.6	1.4
	15.8	596	931	0.64	0.0475	0.0016	0.0867	0.0018	0.0132	0.0002	84.4	1.7	84.7	1.4
	12.9	613	709	0.86	0.0479	0.0018	0.0882	0.0023	0.0134	0.0002	85.8	2.2	85.5	1.5
	57.8	360	3955	0.09	0.0478	0.0015	0.0873	0.0016	0.0133	0.0002	85.0	1.5	84.8	1.4
	16.6	636	984	0.65	0.0477	0.0016	0.0868	0.0020	0.0132	0.0002	84.5	1.9	84.6	1.5
	23.0	272	1519	0.18	0.0478	0.0016	0.0882	0.0019	0.0134	0.0002	85.8	1.8	85.8	1.4
	61.9	828	4064	0.20	0.0482	0.0015	0.0894	0.0017	0.0135	0.0002	87.0	1.5	86.3	1.4
	18.3	517	1139	0.45	0.0488	0.0019	0.0897	0.0025	0.0133	0.0002	87.2	2.3	85.3	1.5
	36.3	276	2471	0.11	0.0494	0.0016	0.0908	0.0019	0.0133	0.0002	88.2	1.8	85.3	1.5
	11.0	822	541	1.52	0.0483	0.0020	0.0900	0.0030	0.0135	0.0003	87.5	2.8	86.6	1.6
	14.3	483	839	0.58	0.0479	0.0017	0.0895	0.0021	0.0136	0.0002	87.0	2.0	86.8	1.5
	37.7	344	2566	0.13	0.0486	0.0016	0.0893	0.0018	0.0133	0.0002	86.8	1.7	85.4	1.5
	16.5	363	1058	0.34	0.0480	0.0018	0.0879	0.0023	0.0133	0.0002	85.6	2.1	85.1	1.5
LJS-65 (CMG)	26.9	716	1621	0.44	0.0485	0.0012	0.0918	0.0015	0.0137	0.0002	89.2	1.4	87.9	0.9
	38.0	953	2409	0.40	0.0478	0.0011	0.0879	0.0012	0.0133	0.0001	85.5	1.2	85.3	0.9
	77.5	638	5280	0.12	0.0478	0.0010	0.0881	0.0011	0.0134	0.0001	85.7	1.0	85.5	0.9
	54.8	233	3797	0.06	0.0474	0.0010	0.0876	0.0011	0.0134	0.0001	85.2	1.1	85.8	0.9
	57.1	906	3786	0.24	0.0478	0.0010	0.0881	0.0011	0.0134	0.0001	85.7	1.0	85.5	0.9
	32.3	460	2097	0.22	0.0477	0.0011	0.0902	0.0012	0.0137	0.0001	87.7	1.1	87.7	0.9
	56.6	516	3795	0.14	0.0477	0.0010	0.0892	0.0011	0.0136	0.0001	86.8	1.1	86.8	0.9
	36.7	815	2346	0.35	0.0487	0.0011	0.0903	0.0014	0.0135	0.0001	87.8	1.3	86.1	0.9
	45.5	486	2961	0.16	0.0480	0.0012	0.0899	0.0017	0.0136	0.0002	87.4	1.6	86.9	0.9
	94.8	976	6386	0.15	0.0482	0.0010	0.0893	0.0010	0.0134	0.0001	86.9	1.0	86.1	0.9
	33.6	526	2232	0.24	0.0486	0.0012	0.0901	0.0016	0.0134	0.0002	87.6	1.5	86.1	0.9
	29.3	445	1932	0.23	0.0478	0.0011	0.0890	0.0013	0.0135	0.0001	86.6	1.2	86.4	0.9
	28.9	603	1896	0.32	0.0480	0.0011	0.0879	0.0013	0.0133	0.0001	85.5	1.2	85.1	0.9
	52.9	787	3449	0.23	0.0488	0.0011	0.0921	0.0013	0.0137	0.0002	89.4	1.2	87.5	0.9
	32.5	907	2044	0.44	0.0483	0.0012	0.0896	0.0015	0.0135	0.0002	87.1	1.4	86.2	0.9

of granites are characterized as strong peraluminous S-type granites.

These granites have high contents of total alkalis (K_2O + Na_2O greater than 5.7 wt%) resulting from strong fractionation, but lower Zr + Nb + Y + Ce contents. Most samples plotted in Fig. 9 fall within the fractionated granite field (Fig. 9). A similar correlation is noted between some selected major and minor elements and SiO_2 (Fig. 7), suggesting that the two granite types were generated during significant fractionation of a homologous magma.

Granite generated from the partial melting of amphibolite in a water-rich environment or the fractional crystallization of aluminous-poor magma, has a medium Al content and a high Sr and Na contents (Gaudemer et al., 1988), which is inconsistent with the geochemical features of the Laojunshan granites. Meanwhile, mica-poor metapsammites or orthogneiss probably could not form strongly peraluminous and SiO_2-rich granite at a low to medium temperature (Beard and Lofgren, 1991). Zircon saturation temperatures calculated by bulk rock compositions can provide useful estimate of initial magma temperatures. The thermometer requires the following factors: (1) Intermediate to felsic magmas. (2) Melt saturated in zircon. Mineralogical and geochemical studies show that Laojunshan granites belong to highly fractionated S-type granite. Abundantly magmatic zircon grains have been observed in the granites show that those melts contained sufficient Zr for saturation in zircon. Thus, the thermometer could be used to estimate the initial magma temperatures of Laojunshan. Zircon saturation temperatures of twenty-six samples calculated by formula of Watson and Harrison (1983) are higher than 800 °C, and ten samples are lower than 800 °C. These calculated temperatures are consistent with the estimated temperatures of the CaO/Na_2O and Al_2O_3/TiO_2

Table 3
Major (wt%) and trace (ppm) element compositions of the Laojunshan granites in SE Yunnan.

Sample	LJS-19	LJS-20	LJS-21	LJS-22	LJS-42	LJS-43	LJS-44	LJS-45	LJS-46	LJS-47	LJS-48	LJS-49	LJS-50	LJS-51	LJS-52	LJS-53	LJS-54	LJS-55
Llithology	FMG				CMG													
SiO_2	72.9	72.9	73.5	72.7	73.7	73.5	73.9	73.1	73.7	73.2	72.9	73.8	73.3	72.7	73.0	73.4	73.3	69.1
Al_2O_3	15.5	15.7	15.1	15.7	13.4	13.9	13.7	14.8	14.8	14.4	14.4	14.9	15.3	15.0	15.4	15.6	15.1	18.1
TFe_2O_3	1.16	1.92	1.42	1.26	1.04	1.47	1.08	1.49	1.44	1.51	1.59	1.02	1.43	1.37	1.30	0.92	0.95	1.36
MgO	0.20	0.23	0.24	0.20	0.33	0.36	0.13	0.25	0.29	0.31	0.23	0.13	0.26	0.24	0.22	0.08	0.11	0.23
CaO	0.92	0.78	0.32	0.74	0.49	0.72	0.39	0.38	0.41	0.77	0.83	0.61	0.51	0.87	0.30	0.39	0.42	0.36
Na_2O	1.42	1.42	2.09	1.66	1.91	2.01	2.80	2.40	2.53	2.75	3.01	1.52	2.15	2.84	1.90	3.15	3.14	0.23
K_2O	4.65	4.32	4.66	4.56	6.30	6.36	4.08	4.70	4.45	4.39	3.21	4.56	5.55	5.41	5.46	4.67	4.67	5.94
MnO	0.05	0.15	0.04	0.09	0.07	0.10	0.08	0.07	0.05	0.08	0.13	0.07	0.03	0.03	0.03	0.07	0.07	0.04
P_2O_5	0.44	0.27	0.22	0.19	0.20	0.22	0.19	0.21	0.22	0.25	0.54	0.48	0.13	0.21	0.11	0.27	0.29	0.33
TiO_2	0.12	0.16	0.17	0.16	0.13	0.13	0.11	0.20	0.20	0.20	0.17	0.09	0.15	0.15	0.16	0.05	0.07	0.17
LOI	2.64	3.10	1.82	2.76	1.86	2.00	1.88	1.38	1.25	1.53	2.14	2.35	1.86	1.27	1.95	1.68	1.45	4.37
total	100.04	100.96	99.60	100.03	99.36	100.83	98.34	98.98	99.40	99.36	99.14	99.49	100.65	100.11	99.76	100.34	99.53	100.18
Li	106	820	140	60.5	96.4	125	49.3	101	62.6	172	578	262	196	145	59.2	213	145	141
Be	9.32	49.0	23.4	17.8	10.4	6.27	47.9	22.6	16.2	19.8	7.72	15.2	12.4	17.4	138	136	36.8	22.3
Ga	22.5	28.8	24.7	22.1	20.7	21.9	21.3	21.7	23.8	23.8	30.8	23.4	27.4	26.2	30.1	30.7	29.8	33.1
Rb	372	795	379	377	737	728	320	356	348	385	522	555	469	441	536	740	727	609
Sr	39.2	26.2	51.5	44.9	24.3	32.8	26.3	49.5	26.0	65.8	40.3	20.0	39.1	41.0	36.3	9.70	13.5	28.2
Y	2.58	13.3	9.23	11.8	11.7	11.0	10.6	10.2	13.5	11.5	11.4	8.53	10.5	9.50	6.80	7.10	8.80	6.80
Zr	64.6	83.3	93.4	84.3	70.0	70.6	62.3	98.7	93.2	90.7	88.7	60.0	85.6	85.8	94.8	33.3	35.2	93.2
Nb	25.2	27.0	27.0	25.8	23.1	21.9	19.0	22.5	23.6	27.0	22.6	52.4	22.5	21.7	23.6	41.0	38.8	25.6
In	1.08	1.22	0.19	0.13	0.13	0.17	1.09	0.19	0.20	1.54	0.12	0.13	0.23	0.19	0.28	1.13	1.20	0.23
Sn	25.7	124	17.3	16.3	83.4	117	15.6	23.3	19.6	31.1	129	31.3	35.0	23.6	36.7	93.4	90.6	37.8
Cs	40.2	112	35.7	20.4	71.3	68.6	24.7	35.5	25.1	41.5	126	79.1	42.9	35.5	35.1	83.2	90.9	45.8
Ba	153	142	188	165	314	195	152	271	252	250	94.4	86.1	181	171	182	48.3	56.9	178
La	14.3	26.4	24.8	21.6	17.0	19.6	16.5	30.4	26.4	32.7	24.3	12.0	24.2	23.4	22.3	5.60	7.10	26.1
Ce	31.8	60.2	52.6	48.3	38.1	44.4	33.0	61.8	71.9	67.5	52.8	26.1	46.6	48.8	48.0	11.8	15.2	56.8
Pr	3.38	7.14	5.98	5.25	4.18	4.86	3.81	6.92	7.37	7.18	5.63	2.75	5.98	5.84	5.70	1.29	1.71	6.45
Nd	12.6	28.1	22.4	19.4	15.4	18.2	14.2	25.8	28.7	26.5	21.1	10.1	22.8	23.3	22.1	4.92	6.22	24.9
Sm	2.95	6.56	5.16	4.28	3.31	3.94	2.78	4.95	5.97	4.72	4.08	2.12	5.79	5.85	5.26	1.41	1.55	6.10
Eu	0.31	0.52	0.37	0.31	0.37	0.40	0.25	0.42	0.59	0.45	0.34	0.16	0.46	0.40	0.33	0.10	0.14	0.42
Gd	2.22	5.44	4.03	3.13	2.77	2.89	2.09	3.46	4.52	3.52	3.29	1.94	4.42	4.25	3.80	1.31	1.25	4.30
Tb	0.26	0.80	0.54	0.40	0.43	0.44	0.34	0.49	0.65	0.49	0.45	0.33	0.64	0.59	0.57	0.30	0.22	0.56
Dy	0.96	3.57	2.31	1.59	2.31	2.16	1.86	2.25	3.39	2.38	2.26	1.77	2.94	2.46	2.46	1.82	1.44	2.17
Ho	0.12	0.56	0.36	0.25	0.41	0.39	0.37	0.38	0.57	0.44	0.41	0.32	0.39	0.34	0.31	0.29	0.28	0.30
Er	0.23	1.35	0.82	0.58	1.16	0.94	1.11	1.00	1.45	1.17	1.03	0.80	0.94	0.74	0.65	0.72	0.79	0.65
Tm	0.03	0.16	0.10	0.08	0.15	0.13	0.17	0.13	0.21	0.16	0.14	0.12	0.12	0.09	0.08	0.11	0.12	0.08
Yb	0.15	1.12	0.71	0.51	0.98	0.82	1.15	0.89	1.31	1.00	1.01	0.83	0.65	0.56	0.47	0.71	0.79	0.47
Lu	0.02	0.14	0.09	0.08	0.13	0.11	0.16	0.12	0.17	0.14	0.12	0.11	0.10	0.09	0.07	0.11	0.12	0.07
Hf	2.21	2.77	3.12	2.73	2.48	2.29	2.14	3.27	3.59	2.94	2.69	2.40	2.91	3.09	3.38	1.46	1.69	3.47
Ta	5.03	6.75	5.44	4.36	4.77	4.62	3.47	4.21	5.15	5.82	4.66	20.2	4.42	3.41	4.35	17.4	15.1	5.56
W	16.9	35.8	13.1	11.6	21.4	21.2	13.0	16.1	20.9	32.6	43.4	35.3	32.0	227	227	312	206	177
Th	9.5	25.2	21.9	20.9	18.1	17.4	14.8	25.8	28.1	23.8	19.3	11.6	18.6	19.1	22.1	6.11	6.85	23.2
U	8.64	5.24	8.83	7.39	15.0	17.4	10.0	6.50	10.6	13.8	9.56	10.6	7.27	5.63	7.74	8.51	6.77	9.86
ΣREE	69.33	142.06	120.27	105.75	86.69	99.26	77.79	139.00	153.20	148.35	116.96	59.45	116.03	116.71	112.10	30.49	36.93	129.37
Ratio																		
LREE/HREE	16.4	9.8	12.4	15.0	9.4	11.6	9.7	14.9	11.5	15.0	12.4	8.6	10.4	11.8	12.3	4.7	6.4	14.0
La_N/Yb_N	67.9	16.9	25.0	30.4	12.4	17.3	10.3	24.4	14.5	23.5	17.3	10.3	26.7	30.0	34.0	5.7	6.4	39.8
δEu	0.37	0.27	0.25	0.26	0.37	0.36	0.32	0.31	0.35	0.34	0.28	0.24	0.28	0.25	0.23	0.22	0.31	0.25
ACNK	1.47	1.60	1.42	1.50	1.01	1.01	1.27	1.31	1.34	1.22	1.39	1.47	1.23	1.10	1.32	1.27	1.23	1.79
Zircon saturation temperatures (°C)																		
Tzr	809	833	844	834	816	817	806	849	844	841	839	803	835	835	845	843	852	849

Sample	LJS-56	LJS-57	LJS-58	LJS-59	LJS-60	LJS-61	LJS-62	LJS-63	LJS-64	LJS-64–2	LJS-65	LJS-66	LJS-68	LJS-69	LJS-70	LJS-71	LJS-72	LJS-73

(*continued on next page*)

Table 3 (*continued*)

Sample	LJS-56	LJS-57	LJS-58	LJS-59	LJS-60	LJS-61	LJS-62	LJS-63	LJS-64	LJS-64–2	LJS-65	LJS-66	LJS-68	LJS-69	LJS-70	LJS-71	LJS-72	LJS-73
Llithology	CMG																	
SiO_2	71.6	72.4	71.3	73.5	73.9	72.5	72.9	74.4	73.7	73.2	73.5	72.0	72.3	72.6	71.6	70.5	73.5	71.7
Al_2O_3	15.4	15.7	16.0	15.4	14.8	16.2	15.7	15.0	14.8	15.5	15.4	15.5	16.2	15.9	17.0	17.5	14.6	15.2
TFe_2O_3	1.49	0.66	1.42	1.24	1.15	1.16	1.28	1.14	0.37	1.56	1.26	1.43	1.27	1.12	1.16	1.16	1.18	1.09
MgO	0.28	0.12	0.26	0.19	0.17	0.14	0.20	0.16	0.05	0.26	0.18	0.28	0.21	0.14	0.15	0.13	0.12	0.17
CaO	0.90	0.42	0.36	0.27	0.90	0.54	0.45	0.36	0.45	0.48	0.57	0.27	0.36	0.33	0.36	0.39	0.36	0.27
Na_2O	2.50	1.89	1.60	2.11	3.24	3.22	2.74	2.70	2.48	2.23	2.20	2.15	2.56	3.04	2.38	3.66	2.55	1.96
K_2O	5.52	5.45	5.84	5.34	4.59	4.48	5.24	4.90	7.25	5.70	5.17	5.83	5.67	4.92	5.15	4.60	4.61	6.75
MnO	0.03	0.02	0.03	0.05	0.06	0.07	0.04	0.06	0.02	0.04	0.03	0.08	0.03	0.06	0.07	0.10	0.06	0.06
P_2O_5	0.30	0.29	0.34	0.21	0.36	0.34	0.33	0.26	0.17	0.17	0.26	0.26	0.25	0.26	0.34	0.23	0.31	0.22
TiO_2	0.20	0.08	0.18	0.11	0.09	0.08	0.10	0.11	0.03	0.17	0.11	0.18	0.14	0.08	0.08	0.07	0.06	0.11
LOI	1.59	2.65	2.60	2.15	1.33	1.87	1.74	1.59	0.92	1.69	2.18	1.81	2.05	2.00	2.43	2.18	2.26	1.76
total	99.88	99.74	99.93	100.60	100.56	100.61	100.69	100.71	100.20	100.95	100.84	99.79	101.00	100.40	100.65	100.46	99.64	99.28
Li	163	340	241	61.8	197	126	74.2	111	162	173	278	222	178	272	235	357	125	56.4
Be	15.2	32.7	36.0	117	16.4	16.4	42.4	21.6	37.2	9.21	7.37	21.8	17.7	5.54	19.5	32.7	33.5	25.7
Ga	27.7	26.9	29.0	27.3	25.9	33.1	28.7	30.5	24.2	29.7	26.6	27.3	27.0	28.9	30.6	30.9	29.1	28.4
Rb	515	486	551	634	583	672	606	638	704	582	489	676	568	720	800	768	722	843
Sr	41.8	25.7	33.1	26.4	32.2	17.5	31.3	29.4	21.1	41.7	31.9	39.7	68.9	16.1	11.1	17.1	13.5	32.1
Y	11.7	5.60	6.30	8.20	12.6	9.40	6.90	13.1	4.01	12.2	7.26	7.75	12.8	6.90	5.23	12.9	6.01	5.33
Zr	102	56.1	89.2	58.5	58.7	38.3	52.9	61.2	35.3	85.6	59.6	99.1	96.2	46.2	48.3	49.3	35.1	62.4
Nb	22.4	16.8	22.7	32.0	29.3	40.8	38.5	41.5	10.2	22.3	20.1	22.7	19.3	29.4	34.9	33.7	39.4	33.2
In	0.21	0.19	0.22	0.54	0.98	1.32	0.67	0.72	0.20	0.36	0.34	0.62	1.02	1.31	1.33	1.53	1.04	0.88
Sn	28.7	23.2	30.6	55.3	85.3	112	54.2	53.8	26.5	29.9	30.2	42.3	50.4	108	99.1	131	101	54.3
Cs	34.5	32.4	41.7	64.4	110	79.6	63.1	60.4	42.2	40.4	28.7	64.2	43.8	126	124	116	97.7	78.6
Ba	203	107	192	111	111	50.2	115	114	44.1	205	128	189	225	79.6	76.3	72.5	67.1	130
La	28.4	10.0	24.5	10.6	12.6	8.40	11.7	17.4	1.50	21.2	17.1	24.1	26.9	8.50	8.00	9.30	7.01	18.2
Ce	63.6	21.8	55.8	22.8	27.3	18.0	25.5	38.1	2.90	47.2	34.2	55.1	58.7	18.1	17.3	21.2	15.5	41.4
Pr	7.08	2.45	6.33	2.42	2.91	1.97	2.81	4.20	0.33	5.46	4.09	6.14	7.08	2.13	2.05	2.57	1.71	4.97
Nd	27.9	9.35	24.3	9.23	11.2	7.36	11.0	16.3	1.28	19.6	14.2	22.9	26.1	7.72	7.56	10.8	6.21	17.7
Sm	6.82	2.25	5.59	2.43	3.04	2.01	3.15	4.06	0.40	4.66	3.08	5.06	6.06	2.02	1.99	3.30	1.47	3.77
Eu	0.44	0.24	0.36	0.20	0.23	0.11	0.26	0.24	0.10	0.33	0.31	0.32	0.46	0.17	0.18	0.34	0.12	0.24
Gd	4.68	1.81	3.84	2.29	3.00	1.76	2.93	3.30	0.48	3.93	2.36	3.61	5.04	1.52	1.46	3.30	1.15	2.74
Tb	0.64	0.31	0.49	0.40	0.53	0.33	0.44	0.54	0.09	0.55	0.32	0.46	0.67	0.26	0.23	0.57	0.21	0.35
Dy	2.93	1.38	1.97	2.05	2.65	1.92	1.84	2.77	0.58	2.69	1.51	2.02	3.11	1.57	1.18	3.33	1.23	1.63
Ho	0.40	0.20	0.27	0.30	0.42	0.32	0.27	0.44	0.11	0.38	0.21	0.29	0.43	0.27	0.18	0.54	0.23	0.22
Er	0.93	0.51	0.59	0.70	1.01	0.85	0.64	1.15	0.30	0.90	0.50	0.60	0.93	0.66	0.46	1.33	0.59	0.48
Tm	0.13	0.07	0.08	0.10	0.15	0.13	0.09	0.18	0.05	0.12	0.07	0.08	0.12	0.09	0.07	0.18	0.09	0.06
Yb	0.73	0.41	0.45	0.64	0.92	0.84	0.55	1.19	0.31	0.70	0.50	0.54	0.74	0.61	0.48	1.11	0.58	0.38
Lu	0.11	0.06	0.07	0.10	0.14	0.13	0.08	0.16	0.05	0.10	0.08	0.09	0.12	0.10	0.08	0.17	0.09	0.06
Hf	3.71	2.11	3.37	2.26	2.33	1.69	2.18	2.31	1.53	2.91	2.03	3.28	3.30	2.00	1.92	1.95	1.53	2.43
Ta	4.02	4.77	4.74	8.53	8.62	13.9	10.9	11.6	1.50	3.02	3.42	5.41	4.53	11.7	12.5	14.2	16.4	15.4
W	179	155	232	167	229	269	202	211	215	167	393	136	226	281	142	209	412	331
Th	29.0	10.1	24.5	9.77	10.2	9.33	10.4	15.8	1.39	19.9	14.7	22.3	25.3	8.67	8.66	8.78	7.29	19.1
U	8.25	3.24	7.70	5.79	6.13	8.38	5.31	8.94	2.86	5.18	5.84	5.73	11.7	6.45	6.38	8.65	6.82	6.35
ΣREE	144.79	50.84	124.64	54.26	66.10	44.13	61.26	90.03	8.48	107.82	78.53	121.31	136.46	43.72	41.22	58.04	36.18	92.20
Ratio																		
LREE/HREE	12.7	9.7	15.1	7.2	6.5	6.0	8.0	8.3	3.3	10.5	13.1	14.8	11.2	7.6	8.9	4.5	7.7	14.6
La_N/Yb_N	27.9	17.5	39.1	11.9	9.8	7.2	15.3	10.5	3.5	21.7	24.5	32.0	26.1	10.0	12.0	6.0	8.7	34.4
δEu	0.24	0.36	0.24	0.26	0.23	0.18	0.26	0.20	0.70	0.24	0.35	0.23	0.25	0.30	0.32	0.31	0.28	0.23
ACNK	1.15	1.34	1.34	1.32	1.14	1.32	1.24	1.26	0.95	1.22	1.28	1.24	1.25	1.28	1.43	1.36	1.29	1.11
Zircon saturation temperatures (°C)																		
Tzr	847	752	756	797	839	800	800	763	790	804	756	835	801	779	783	785	756	805

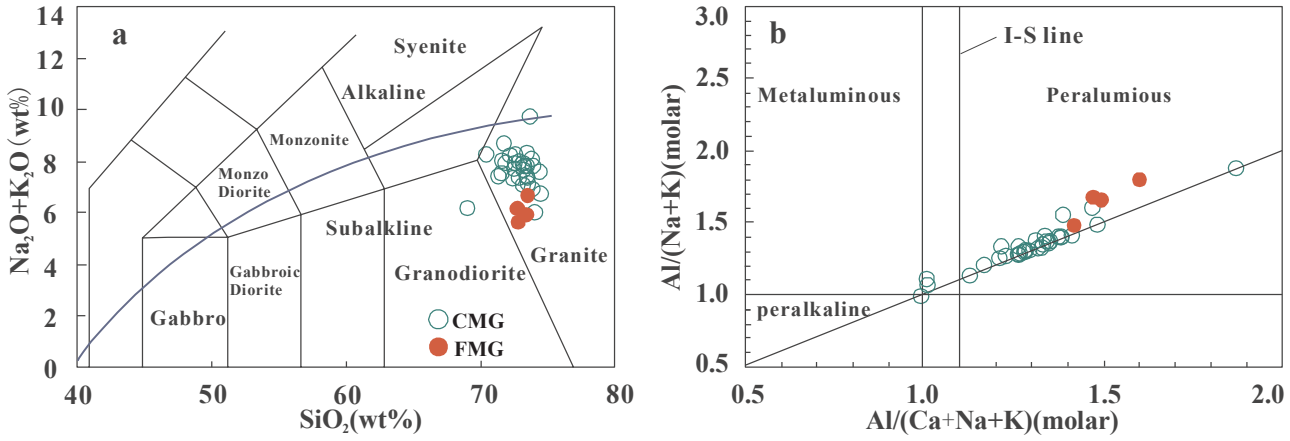

Fig. 5. (a) (K_2O + Na_2O) vs. SiO_2 (Middlemost, 1994) and (b) molar Al/(Na + K) vs. molar Al/(Ca + Na + K) plots for the Laojunshan granites.

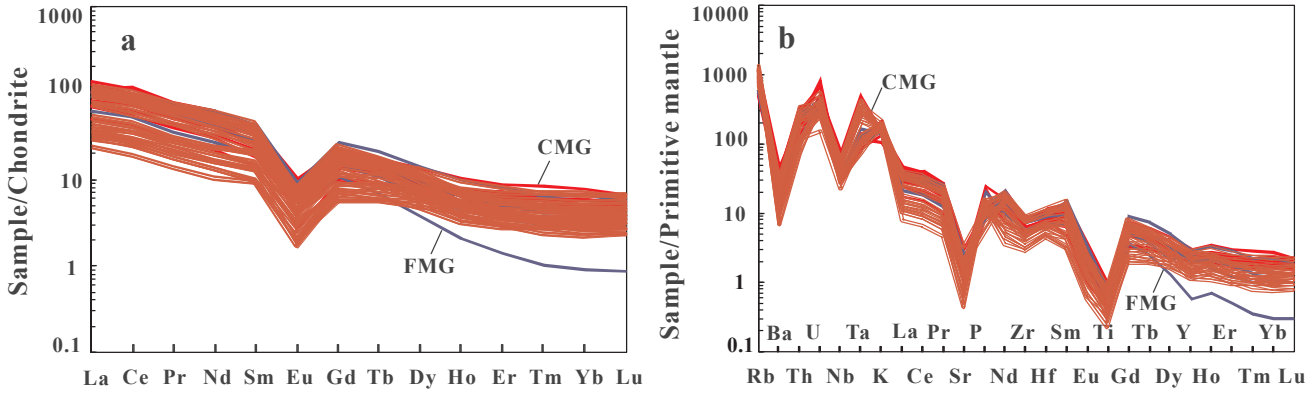

Fig. 6. (a) Chondrite-normalized REE pattern and (b) primitive mantle-normalized spidergram for Laojunshan granites. The chondrite and primitive-mantle data are from Sun and McDonough (1989).

diagrams (Sylvester, 1998), reflecting lower initial magma temperatures. Thus, Laojunshan granitic magma could be derived from the partial melting of the Al-rich metamorphic basement in the middle or lower crust. This theory is also supported by the lithology of the basement rock in the Laojunshan region (basement rock consists mainly of schist) and high Rb contents in the granites (Fig. 6b).

Generally, CaO/Na_2O ratio lower than 0.3 is indicative of granite derived from the metapelite source, while CaO/Na_2O ratio higher than 0.3 show granite derived from the metapsammite source (Chappell and White, 1992). In Fig. 10, the CaO/Na_2O ratios of twenty-eight samples are lower than 0.3 and those of eight samples are higher than 0.3. These geochemical features suggest that the Laojunshan granites likely originated from plagioclase-poor and clay-rich sources (Chappell and White, 1992; Sylvester, 1998). In addition, both granite types have comparatively higher Rb/Sr and Rb/Ba ratios and fall within the politic-rich field (Fig. 10b).

The Hf isotopic compositions of zircon grains in Laojunshan granites have relatively large variation with the εHf(t) varying from −12.88 to −1.19 (Fig. 8), while the two-stage Hf model ages range from 1.2 Ga to 1.9 Ga. In the zircon $\varepsilon_{Hf}(t)$ values vs. age diagram, Laojunshan granite samples plotted below the depleted mantle and the Chondrite evolution line and they fallen in the crust Hf isotope evolution line from about 1.97 to 1.23 Ga (Fig. 8), indicating that the granites likely originated from partial melting of the preexisting crust materials separated from depleted mantle sources during the Mesoproterozoic to Paleoproterozoic (Liu et al., 2006).

5.2. Late Cretaceous magma fractionation

In the log–log diagrams of Ba vs. Eu, Sr vs. Eu and Ba vs. Sr (Fig. 11), the variation in the trends exhibited by the elements show that there is extensive fractionation of plagioclase and K-feldspar. The plagioclase fractional crystallization can lead to the depletion of Sr and Eu (Fig. 6 a, b), while the separation of K-feldspar can result in the depletion of Ba and Eu (Fig. 6a, b). In addition, the high Rb/Sr ratios in the Laojunshan granites also illustrate the fractionation of plagioclase in the magma evolution (Fig. 10b; Bouseilly and Sokkary, 1975). The La and Yb contents of the granites seem to be influenced by the several-degree fractional crystallization of allanite or monazite, while the negative correlation between TiO_2 and SiO_2 (Fig. 7) and the depletion of Ti (Fig. 6b) suggest the fractionation of ilmenite or biotite.

5.3. In-, Sn- and W-enrichment and its relationship with the granites

The western Cathaysia block is the most concentrated area of W–Sn–In polymetallic ore deposits in the world (Hua and Mao, 1999; Mao et al., 1999,2013). From west to east, the Gejiu Sn–Cu–In polymetallic deposit in Gejiu ore concentrated area, Bainiuchang Ag–Sn–In deposit in Bozhushan ore concentrated area, Dulong Sn–In polymetallic deposit and Nanyangtian W–B deposit in Laojunshan ore concentrated area are successively distributed in SE Yunnan (Tu, 2002, Wang et al., 2019). The metallogenic ages obtained several analytical methods for Gejiu deposit range from 77.4 ± 0.6 Ma to 95.4 ± 0.7 Ma (Table 1; Cheng, 2012). LA-MC-ICP-MS cassiterite U–Pb ages for Bainiuchang deposit range from 87.4 ± 3.7 Ma to 88.4 ± 4.3 Ma (Table 1; Li et al., 2013c,b). The muscovite and bitote Ar–Ar ages of the Nanyangtian W–B

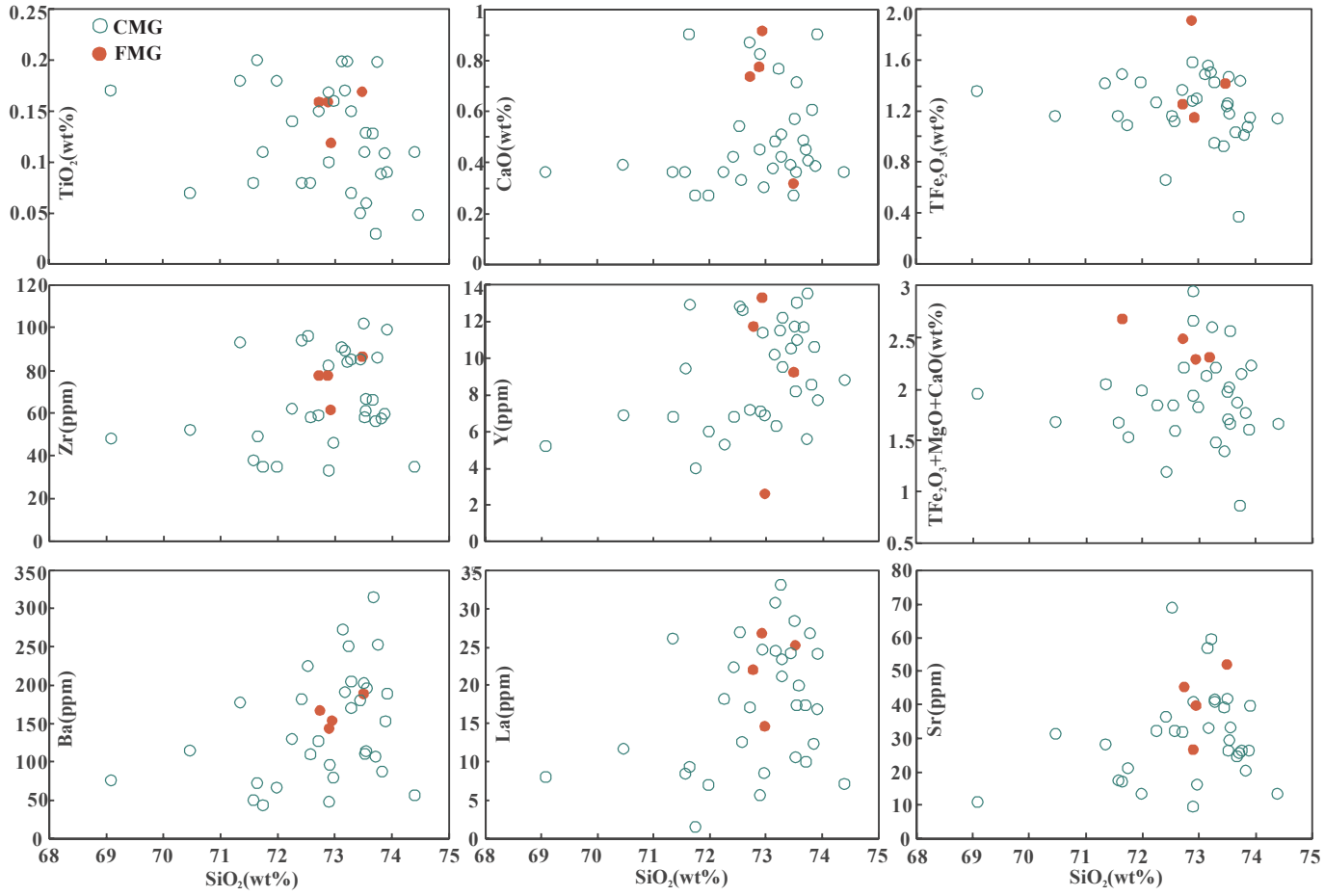

Fig. 7. Major and trace elements variation diagrams for Laojunshan granites.

polymetallic deposit are from 97.49 ± 0.97 Ma to 118.14 ± 0.69 Ma (Liu et al., 2011; Wang et al., 2019). The mica Ar–Ar and molybdenite Re–Os ages of Dulong deposit obtained by Li et al (2013b) are from 75.04 ± 1.78 Ma to 93.6 ± 1.1 Ma, and the TIMS and LA-MC-ICP-MS cassiterite U–Pb dating are from 87.2 ± 3.9 Ma to 89.2 ± 4.1 Ma (Table 1; Liu et al., 2007; Wang et al., 2014). Recently published geochronological data and ages of this study (85.6 ± 0.8 Ma to 90.37 ± 0.77 Ma) on granites indicate that the granites in the western Cathaysia block are mainly from 77 Ma to 117 Ma. Thus deposits in SE Yunnan are closely related to granites both spatially and temporally (Table 1; Qin et al., 2006; Yang et al., 2008; Liu et al., 2007; Cheng et al., 2008, 2009,2010a,2010b, Cheng and Mao, 2010; Cheng, 2012; Li et al., 2013b, c, d; Wang et al., 2014).

W, Sn, In, Li and Be contents in Laojunshan granites are from 11.60 ppm to 43.40 ppm, 15.56 ppm to 129.21 ppm, 0.13 ppm to 1.53 ppm, 49.35 ppm to 819.85 ppm and 6.27 ppm to 49.04 ppm respectively. They are several times higher than the average content of the upper and lower crust (2 ppm and 0.7 ppm for W, 5.5 ppm and 1.5 ppm for Sn, 20 ppm and 11 ppm for Li and 3.0 ppm and 1.0 ppm for Be) or continental crust (0.05 ppm for In; Rudnick and Gao, 2003) and most granites in South China. The $^{206}Pb/^{204}Pb$, $^{207}Pb/^{204}Pb$ and $^{208}Pb/^{204}Pb$ values of sulfides from Dulong polymetallic deposit are from 18.286 to 18.6967, 15.541 to 15.771 and 38.111 to 39.338, respectively, whereas the Pb isotopic compositions of Laojunshan granites are from 18.264 to 18.662, 15.637 to 15.738 and 38.014 to 39.187 respectively (He et al., 2015). And homogeneous Pb isotope and $\delta^{34}S$ variation (−1.3 to 4.9) for sulfides from Dulong deposit reflect that the metallogenic material mainly origin from granite. And oxygen and hydrogen isotopic compositions of quartz and scheelite from Nanyangtian, Huangtian, Wazha and Saxi tungsten polymetallic deposits show that ore-forming fluids derived from magmatic fluid, which exsolved from Laojunshan granites (Feng et al., 2010; Ye et al., 2016). So the high concentrations of metallogenic elements in Laojunshan granites would provide material preparation for regional deposits. Magmatic crystallization usually leads to silicon and alkalis, F, B, Cl and H_2O increased rapidly in residual phase (Audétat et al., 2000; Thomas et al., 2004). Following the cooling the highly fractionated volatiles-riched Laojunshan granites, where the partitioning of Sn, W, In into crystallization phase are limited, would efficiently removal of Sn, W, and In into a volatile-rich (F, Cl) hydrothermal fluid (Audétat et al., 2000; Thomas et al., 2004). Chemical compositions of In-bearing Pb–Zn ores and fluid inclusions hosted in quartz separated from In-bearing Pb–Zn ores in Dulong deposit show significant positive correlation between In and Sn in ore-forming fluids. Although the intrinsic mechanism needs further study, Sn seems to have the ability to move In from the melt phase into the ore-forming fluids.

5.4. Tectonic setting of Laojunshan granites

The Late Cretaceous igneous rocks are not only distributed in the Laojunshan district but also widespread in the SW Cathaysia block, such as SE Yunnan, western Guangxi and North Vietnam. The geochronological data reported and summarized in this study show that the magmatism in the SW Cathaysia block was of a short duration (77 Ma to 117 Ma with a peak at 80 Ma to 95 Ma). Although extensive geochronological, geochemical and isotopic investigations during the past 20 years, geodynamic setting of Cretaceous granites distributed in the region has remained poorly understood. The following theories were postulated: (1) related to Indian-Eurasian collision or Ailaoshan subduction (Zhang, 2011); (2) flat subduction of the Pacific plate (Liu et al,

Table 4
Zircon Hf isotopic compositions of the CMG and FMG from Laojunshan.

Sample	Ages (Ma)	$^{176}Hf/^{177}Hf$	1SE	$^{176}Yb/^{177}Hf$	1SE	$^{176}Lu/^{177}Hf$	1SE	εHf(0)	εHf(t)	T_{DM1}	T_{DM2}	$f_{Lu/Hf}$
LJS19 (FMG)	92.4	0.282352	0.000015	0.038355	0.000367	0.000934	0.000010	−14.85	−12.88	1269	1967	−0.97
	90.2	0.282469	0.000021	0.050047	0.000196	0.001178	0.000006	−10.72	−8.82	1113	1710	−0.96
	87.6	0.282440	0.000028	0.062530	0.000335	0.001515	0.000007	−11.73	−9.90	1163	1776	−0.95
	87.3	0.282438	0.000020	0.044211	0.000067	0.001078	0.000002	−11.81	−9.96	1153	1779	−0.97
	92.0	0.282413	0.000020	0.049661	0.000146	0.001138	0.000003	−12.71	−10.76	1190	1834	−0.97
	90.0	0.282686	0.000029	0.076177	0.000935	0.001868	0.000024	−3.05	−1.19	821	1226.	−0.94
	90.3	0.282475	0.000018	0.030326	0.000107	0.000760	0.000003	−10.52	−8.59	1092	1695	−0.98
	87.2	0.282559	0.000015	0.024582	0.000747	0.000646	0.000017	−7.54	−5.66	972	1508	−0.98
	90.6	0.282580	0.000020	0.045855	0.000665	0.001123	0.000014	−6.78	−4.86	954	1460	−0.97
	91.0	0.282499	0.000024	0.050766	0.000248	0.001263	0.000006	−9.66	−7.74	1073	1642	−0.96
LJS47 (CMG)	89.1	0.282581	0.000020	0.050990	0.000293	0.001302	0.000007	−6.74	−4.86	957	1459	−0.96
	89.6	0.282635	0.000033	0.083948	0.000122	0.002082	0.000002	−4.85	−3.01	900	1342	−0.94
	90.6	0.282555	0.000015	0.035988	0.000339	0.000909	0.000007	−7.69	−5.76	985	1517	−0.97
	90.1	0.282544	0.000024	0.063596	0.000215	0.001679	0.000004	−8.07	−6.20	1020	1544	−0.95
	90.4	0.282623	0.000031	0.067442	0.001090	0.001735	0.000024	−5.29	−3.41	909	1367	−0.95
	90.1	0.282509	0.000016	0.028133	0.000287	0.000726	0.000006	−9.29	−7.36	1043	1617	−0.98
	92.1	0.282619	0.000023	0.089618	0.000189	0.002170	0.000008	−5.43	−3.54	926	1377	−0.93
	91.8	0.282590	0.000020	0.045102	0.000671	0.001119	0.000015	−6.45	−4.51	940	1438	−0.97
	91.2	0.282588	0.000019	0.032378	0.000269	0.000844	0.000008	−6.50	−4.55	936	1441	−0.97
	91.5	0.282520	0.000020	0.029676	0.000149	0.000784	0.000004	−8.91	−6.95	1029	1593	−0.98
	89.1	0.282589	0.000033	0.064681	0.000776	0.001636	0.000018	−6.48	−4.62	955	1444	−0.95
	92.2	0.282550	0.000017	0.033019	0.000402	0.000835	0.000009	−7.84	−5.87	988	1525	−0.97
	87.1	0.282518	0.000023	0.167867	0.002440	0.003757	0.000051	−8.99	−7.29	1120	1610	−0.89
	90.2	0.282558	0.000023	0.131667	0.002130	0.003018	0.000050	−7.58	−5.78	1038	1517	−0.91
	91.4	0.282501	0.000017	0.020631	0.000040	0.000507	0.000001	−9.59	−7.61	1049	1635	−0.98
LJS53 (CMG)	86.2	0.282588	0.000023	0.035510	0.000277	0.001076	0.000007	−6.52	−4.69	942	1446	−0.97
	85.6	0.282599	0.000017	0.026601	0.000173	0.000827	0.000004	−6.13	−4.30	920	1420	−0.98
	84.7	0.282492	0.000018	0.042556	0.000409	0.001327	0.000012	−9.89	−8.11	1084	1661	−0.96
	85.5	0.282522	0.000023	0.068287	0.001270	0.002098	0.000036	−8.84	−7.09	1064	1596	−0.94
	84.8	0.282405	0.000017	0.054898	0.000201	0.001726	0.000006	−12.98	−11.21	1220	1856	−0.95
	84.6	0.282593	0.000019	0.019982	0.000139	0.000638	0.000004	−6.34	−4.52	924	1434	−0.98
	85.8	0.282584	0.000021	0.024162	0.000073	0.000761	0.000002	−6.64	−4.81	939	1453	−0.98
	86.3	0.282505	0.000021	0.045032	0.000235	0.001401	0.000010	−9.45	−7.64	1068	1632	−0.96
	85.3	0.282577	0.000021	0.033478	0.000399	0.001007	0.000013	−6.89	−5.07	955	1469	−0.97
	85.3	0.282492	0.000018	0.027873	0.000139	0.000874	0.000006	−9.91	−8.09	1071	1660	−0.97
	86.6	0.282493	0.000020	0.011866	0.000024	0.000364	0.000001	−9.85	−7.97	1055	1654	−0.99
	86.8	0.282588	0.000020	0.023776	0.000054	0.000768	0.000004	−6.49	−4.63	933	1443	−0.98
	85.4	0.282585	0.000020	0.027988	0.000152	0.000844	0.000003	−6.63	−4.75	941	1451	−0.97
	85.1	0.282492	0.000018	0.027873	0.000139	0.000874	0.000006	−9.91	−8.09	1071	1660	−0.97
LJS65 (CMG)	87.9	0.282583	0.000019	0.050423	0.000337	0.001273	0.000008	−6.68	−4.83	954	1455	−0.96
	85.3	0.282583	0.000018	0.060412	0.000392	0.001535	0.000010	−6.67	−4.89	960	1457	−0.95
	85.5	0.282619	0.000015	0.027995	0.000165	0.000717	0.000004	−5.42	−3.59	890	1375	−0.98
	85.8	0.282494	0.000014	0.064328	0.000507	0.001635	0.000012	−9.85	−8.06	1091	1658	−0.95
	85.5	0.282598	0.000019	0.071787	0.000119	0.001759	0.000004	−6.14	−4.37	944	1424	−0.95
	87.7	0.282643	0.000016	0.049825	0.000196	0.001255	0.000006	−4.57	−2.71	868	1322	−0.96
	86.8	0.282545	0.000014	0.039221	0.000085	0.000994	0.000002	−8.04	−6.20	1001	1541	−0.97
	86.1	0.282671	0.000018	0.078929	0.001810	0.001952	0.000044	−3.57	−1.79	844	1262	−0.94
	86.9	0.282569	0.000018	0.058699	0.000133	0.001386	0.000004	−7.18	−5.36	977	1488	−0.96
	86.1	0.282644	0.000029	0.057641	0.000328	0.001456	0.000007	−4.54	−2.74	872	1322	−0.96
	86.1	0.282508	0.000020	0.062621	0.000659	0.001612	0.000018	−9.34	−7.54	1070	1626	−0.95
	86.4	0.282529	0.000026	0.047288	0.000430	0.001157	0.000009	−8.60	−6.77	1027	1577	−0.97
	85.1	0.282585	0.000021	0.052344	0.000337	0.001265	0.000008	−6.63	−4.84	951	1454	−0.96
	87.5	0.282581	0.000020	0.040452	0.000238	0.001010	0.000007	−6.74	−4.88	949	1459	−0.97
	86.2	0.282587	0.000019	0.067558	0.000350	0.001639	0.000008	−6.53	−4.73	957	1448	−0.95

2007; Zhang et al., 2013). It seems impossible to explain the magma related to Indian-Eurasian collision, because it is inconsistent with the previous knowledge that the collision time of the India-Eurasian is 65 Ma (Mo et al., 2003; Wang et al., 2003; Cheng, 2012). It is generally accepted that large volume magma in South China is associated with Pacific plate subduction (Zhou et al., 2006; Sun et al., 2007). However pronounced phenomenons include SE Yunnan is far away from subduction zone (more than 1500 km; Espurt et al., 2008), NE trending subduction zone is inconsistent with the NW trending granitic bodies in SE Yunnan and Pacific plate retreated in the Late Cretaceous (Xia et al., 2016), which consistently show a weak influence of Pacific plate subduction on SE Yunnan.

Cretaceous magma in SE Yunnan is more strongly influenced by the Tethys tectonic domain. Widespread mafic or ultramafic rocks along the China–Vietnam border (Zhang et al., 2003a,2003b) have been diagnosed as having mid-oceanic ridge features (Wu et al., 2002). Ophiolite has been found in the Malipo County of SE Yunnan (Zhong et al., 1998), which has the Sm–Nd isochronous age of 328 Ma. Regional stratigraphic comparative and paleontological studies suggest that the research area is part of the Tethyan Ocean in Permian. Zhang et al. (2006) named this ocean after the Dian-Qiong Ocean. The Dian-Qiong oceanic crust was subducted underneath the Indochina block in the Late Permian to Middle Triassic, then collided in the Late Triassic (Roger et al., 2000; Cai and Zhang, 2009) and formed the Ailao Shan-Song Ma sutures. Subsequently, the tectonic environment transformed into an extensional setting in the Late Cretaceous (Zhou and Li, 2000; Niu, 2005; Xu and Xie, 2005). The extensional tectonic is recorded by the Laojunshan metamorphic core complex (which is a northern part of Song Chay Dome), and a series of large-scale highly active glide faults (Fig. 2; Wen-Ma, Tian-Pan, Maguan-Dulong faults) and the rift-basins

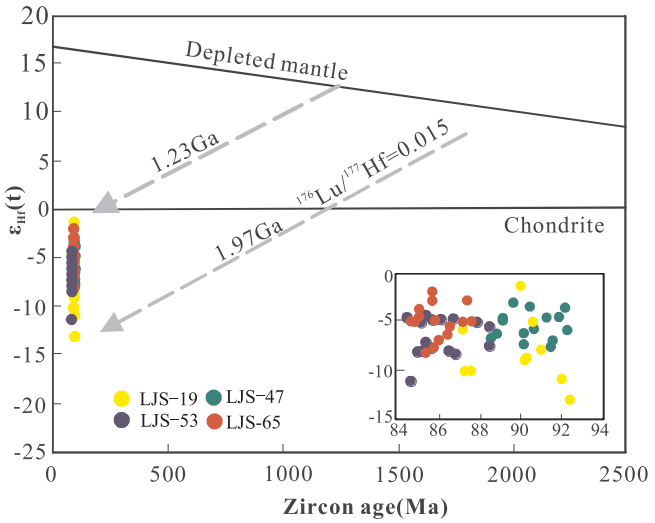

Fig. 8. Zircon $\varepsilon_{Hf}(t)$ values vs. age diagram for CMG and FMG.

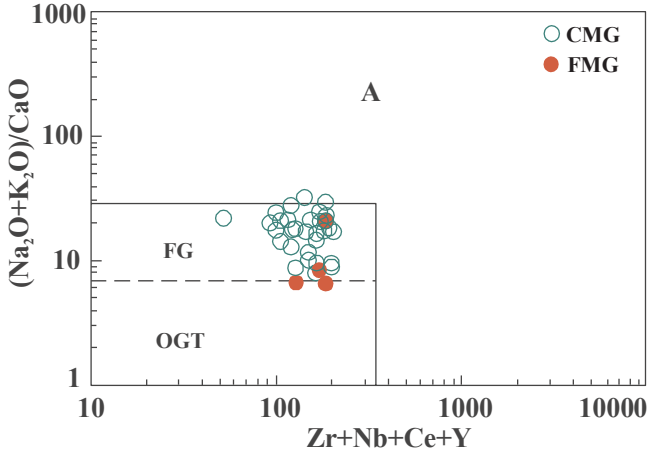

Fig. 9. Zr + Nb + Ce + Y vs. $(Na_2O + K_2O)/CaO$ diagram of Laojunshan granites (Whalen et al., 1987). FG = fractionated I-type granite; OGT = unfractionated I-S-M type granite.

(Neogene sedimentary basins in Maguan and Wenshan counties) in the western Cathaysia block (Roger et al., 2000; Maluski et al., 2001; Yan et al., 2005; Liu et al., 2011; Zhang et al., 2009). The Cretaceous-Neogene alkaline basic rocks exposed in SE Yunnan also reflect the intraplate extensional tectonic environment (Huang et al., 2018). Large-scale extensional tectonic in SE Yunnan is still documented by the seismic data, which reveal that the lithosphere in the region is thinner than peripheral region (Zhao et al., 1992). Even though the extensional peak in the region occurred in Cretaceous, the regionally active tectonic movements were related to extension until recent times. Delamination may be the main mechanism for the change of the tectonic background. Lithospheric extension is often accompanied by upwelling of the asthenosphere and underplating of the mantle-derived magma (Sun et al., 2011), which subsequently may have led to the partial melting of metamorphosed pelitic rocks in the lower crust to form S-type granite.

6. Conclusions

(1) The emplacement ages of granites in the Laojunshan district fall within the range from 85.6 ± 0.8 Ma to 90.37 ± 0.77 Ma. The majority of granites are silica rich and strongly peraluminous S-type granites. The geochemical and isotopic results reveal that the Laojunshan granites originated from the partial melting of the Al-rich metamorphic basement.

(2) The depletion of Ba, Sr and Eu and the relatively higher Rb/Sr ratios of the granites are indicative of fractional crystallization of the plagioclase during magma evolution. The contents of La, Yb and Ti in the granites seem to be controlled by the fractional crystallization of allanite, monazite, ilmenite or other accessory minerals. Metallic elements such as W, Sn, In, Li and Be are enriched in the hydrothermal fluid due to their incompatible properties.

(3) Widespread granites and occurrences of world-class W–Sn–In polymetallic deposits in SE Yunnan are a response to the strong extension of the lithosphere in the Late Cretaceous. The Laojunshan granites formed in the post-collision setting and may mark the onset of lower crust delamination.

Declaration of Competing Interest

The authors declare that they have no known competing financial interests or personal relationships that could have appeared to influence the work reported in this paper.

Acknowledgements

This study was jointly supported by the National Key Research and Development Program of China (2017YFC0602500) and National Natural Science Foundation of China (NSFC) project (41663006, 41572060 and 41762008). We obtained particular guidance and assistance from Bao Guangping for major and trace elements analyses at State Key Laboratory of Ore Deposit Geochemistry and Prof. Yuan Honglin for Zircon U–Pb dating and in situ zircon Hf isotope analyses at State Key Laboratory of Continental Dynamics. We appreciate Dr. Abdul Ghaffar vary much for helping with language modification and the

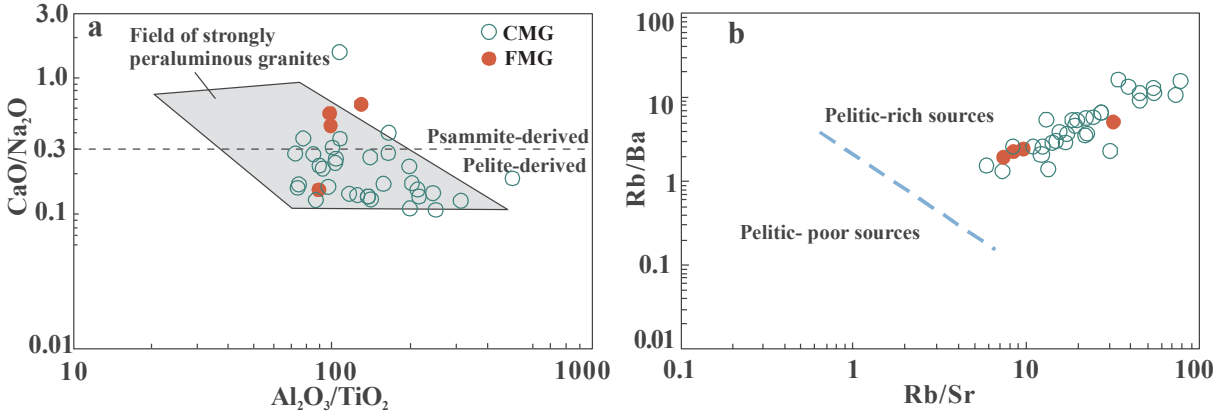

Fig. 10. (a) Al_2O_3/TiO_2 vs. CaO/Na_2O (b) Rb/Sr vs. Rb/Ba diagrams (Sylvester, 1998) for Laojunshan granites.

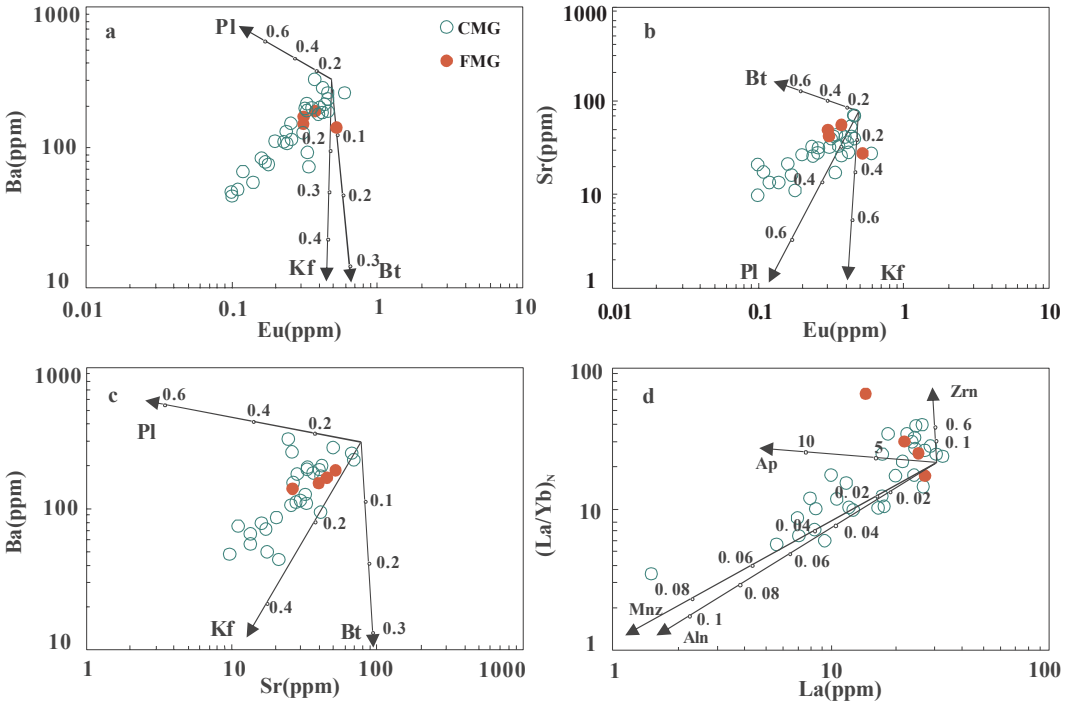

Fig. 11. (a) Ba vs. Eu, (b) Sr vs. Eu, (c) Ba vs. Sr and (d) $(La/Yb)_N$ vs. La diagrams for Laojunshan granites. Partition coefficients are from Mahood and Hildreth (1983) for zircon and allanite; Rollinson (1993) for Ba, Sr and Eu; Fujimaki (1986) for apatite; and Yurimoto et al. (1990) for monazite. Pl = plagioclase; Kf = K-feldspar; Bt = biotite; Aln = allanite; Mnz = monazite; Ap = apatite; Zrn = zircon.

suggestions on our manuscript.

References

Amelin, Y., Lee, D.C., Halliday, A.N., 2000. Early-middle archaean crustal evolution deduced from Lu-Hf and U-Pb isotopic studies of single zircon grains. Geochim. Cosmochim. Acta 64 (16), 4205–4225.

Audétat, A., Gäther, D., Heinrich, C.A., 2000. Magmatic-hydrothermal evolution in a fractionating granite: A microchemical study of the Sn-W-F-mineralized Mole Granite (Australia). Geochim. Cosmochim. Acta 64 (16), 3373–3393.

Beard, J.S., Lofgren, G.E., 1991. Dehydration melting and water-saturated melting of basaltic and andesitic greenstones and amphibolites at 1, 3, and 6.9 kb. J. Petrol. 32 (2), 365–401.

Bi, M.F., Zhang, D., Wu, G.G., Di, Y.J., Que, C.Y., Pan, J.B., Xue, W., 2015. Mesozoic tectonic deformation and ore-controlling of tungsten polymetallic deposits in Malipo area, southeastern Yunnan. Earth Sci. Front. 22 (4), 223–238 (in Chinese with English abstract).

Bouseilly, A.M.E., Sokkary, A.A.E., 1975. The relation between Rb, Ba and Sr in granitic rocks. Chem. Geol. 16 (3), 207–219.

Breiter, K., 2012. Nearly contemporaneous evolution of the A-and S-type fractionated granites in the Krušné hory/Erzgebirge Mts., Central Europe. Lithos 151 (15), 105–121.

Cai, J.X., Zhang, K.J., 2009. A new model for the Indochina and South China collision during the Late Permian to the Middle Triassic. Tectonophysics 467 (1–4), 35–43.

Chappell, B.W., White, A.J.R., 1992. I- and S-type granites in the Lachlan Fold Belt. Trans. R. Soc. Edinb. Earth Sci. 83 (1–2), 1–26.

Cheng, Y.B., Mao, J.W., Xie, G.Q., Chen, M.H., Zhao, C.S., Yang, Z.X., Zhao, H.J., Li, X.Q., 2008. Petrogenesis of the Laochang-Kafang granite in the Gejiu area, Yunnan province: constraints from geochemistry and zircon U-Pb dating. Acta Geol. Sin. 82 (11), 1478–1493 (in Chinese with English abstract).

Cheng, Y.B., Mao, J.W., Xie, G.Q., Chen, M.H., Yang, Z.X., 2009. Zircon U-Pb dating of granites in Gejiu superlarge tin polymetallic orefield and its significance. Miner. Deposits 28 (3), 297–312 (in Chinese with English abstract).

Cheng, Y.B., Mao, J.W., 2010a. Age and geochemistry of granites in Gejiu area, Yunnan province, SW China: constraints on their petrogenesis and tectonic setting. Lithos 120 (3–4), 258–276.

Cheng, Y.B., Tong, X., Wu, J.D., Mo, G.P., 2010a. Geochronology framework of the W-Sn mineralization granites in western South China and their geological significance. Acta Petrol. Sin. 26 (3), 809–818 (in Chinese with English abstract).

Cheng, Y.B., Mao, J.W., Chen, X.L., Li, W., 2010b. LA-ICP-MS zircon U–Pb dating of the Bozhushan granite in southeastern Yunnan province and its significance. J. Jilin Univ. (Earth Sci. Ed.) 40 (4), 869–878 (in Chinese with English abstract).

Cheng, Y.B., 2012. Spatial-temperal evolution of the magmatism and mineralization in the Gejiu supergiant Sn polymetallic district and insights into several key problems. University of Geosciences for Doctoral Degree. China University of Geosciences, Beijing, pp. 1–340 (in Chinese with English abstract).

Cheng, Y.B., Mao, J.W., Spandler, C., 2013. Petrogenesis and geodynamic implications of the Gejiu igneous complex in the western Cathaysia Block: South China. Lithos 175–176, 213–229.

Deng, J.H., Yang, X.Y., Sun, W.D., Huang, Y., Chi, Y.Y., Yu, L.F., Zhang, Q.M., 2012. Petrology, geochemistry, and tectonic significance of Mesozoic shoshonitic volcanic rocks, Luzong volcanic basin, eastern China. Int. Geol. Rev. 54 (6), 714–736.

Espurt, N., Funiciello, F., Martinod, J., Guillaume, B., Regard, V., Faccenna, C., Brusset, S., 2008. Flat subduction dynamics and deformation of the South American plate: Insights from analog modeling. Tectonics 27 (3), 1–19.

Feng, J.R., Mao, J.W., Pei, R.F., Zhou, Z.H., Yang, Z.X., 2010. SHRIMP zircon U-Pb dating and geochemical characteristics of Laojunshan granite intrusion from the Wazha tungsten deposit, Yunnan province and their implications for petrogenesis. Acta Petrol. Sin. 26 (3), 845–857 (in Chinese with English abstract).

Fujimaki, H., 1986. Partition coefficients of Hf, Zr, and REE between zircon, apatite, and liquid. Contrib. Mineral. Petrol. 941 (1), 42–45.

Gaudemer, Y., Jaupart, C., Tapponnier, P., 1988. Thermal control on post-orogenic extension in collision belts. Earth Planet. Sci. Lett. 89 (1), 48–62.

Griffin, W.L., Wang, X., Jackson, S.E., Pearson, N.J., O'Reilly, S.Y., Xu, X.S., Zhou, X.M., 2002. Zircon chemistry and magma mixing, SE China, in-situ analysis of Hf isotopes. Tonglu and Pingtan igneous complexes. Lithos 61 (3–4), 237–269.

He, F., Zhang, Q., Liu, Y.P., Ye, L., Miao, Y.L., Wang, D.P., Su, H., Bao, T., Wang, X.J., 2015. Lead isotope compositions of Dulong Sn–Zn polymetallic deposit, Yunnan, China: constraints on ore-forming metal sources. Acta Mineral. Sin. 35 (3), 309–317 (in Chinese with English abstract).

Hoskin, P.W.O., Schaltegger, U., 2003. The composition of zircon and igneous and metamorphic petrogenesis. Rev. Mineral. Geochem. 53 (1), 27–62.

Hu, Z.L., Yang, X.Y., Duan, L.A., Sun, W.D., 2014. Geochronological and geochemical constraints on genesis of the adakitic rocks in Outang, South Tan-Lu fault Belt (Northeastern Yangtze Block). Tectonophysics 626, 86–104.

Hua, R.M., Mao, J.W., 1999. A preliminary discussion on the Mesozoic metallogenic explosion in east China. Miner. Deposits 18 (4), 300–307 (in Chinese with English abstract).

Hua, R.M., Zhang, W.L., Gu, S.Y., Chen, P.R., 2007. Comparison between REE granite and W-Sn granite in the Nanling region, South China, and their mineralizations. Acta Petrol. Sin. 23 (10), 2321–2328 (in Chinese with English abstract).

Hua, R.M., Li, G.L., Zhang, W.L., Hu, D.Q., Chen, P.R., Chen, W.F., Wang, X.D., 2010. A tentative discussion on differences between large-scale tungsten and tin mineralizations in South China. Miner. Deposits 29 (1), 9–23 (in Chinese with English abstract).

Huang, W.L., Xu, J.F., Chen, J.L., Huang, F., Pi, Q.H., Li, Z.L., 2018. Geochronology, geochemistry and genesis of the baiyunshan alkalic rocks in gejiu area of southeastern Yunnan province. Acta Petrol. Miner. 37 (5), 716–732 (in Chinese with English abstract).

Jackson, S.E., 2008. LAMTRACE data reduction software for LA-ICP-MS. Mineralogical Association of Canada Short Course Series 40, 305–307.

Lan, J.B., Liu, Y.P., Ye, L., Zhang, Q., Wang, D.P., Su, H., 2016. Geochemistry and age spectrum of Late Yanshanian granites from Laojunshan area, southeastern Yunnan

province. China. Acta Mineral. Sin. 36 (4), 441–454 (in Chinese with English abstract).
Li, J.K., Wang, D.H., Li, H.Q., Chen, Z.H., Mei, Y.P., 2013a. Late Jurassic-Early Cretaceous mineraliztion in the Laojunshan ore concentration area, Yunnan province. Earth Sci.-J. China Univ. Geosci. 38 (5), 1023–1036 (in Chinese with English abstract).
Li, J.W., Pei, R.F., Wang, Y.L., She, H.Q., Feng, C.Y., Guo, Z.J., Wang, H.L., Xu, K., 2013b. Isotopic chronological studies of Dulong tin-zinc deposit in Yunnan province. Miner. Deposits 32 (4), 767–782 (in Chinese with English abstract).
Li, K.W., Zhang, Q., Wang, D.P., Cai, Y., Zhang, Y.B., 2013c. New understanding on lead isotopic compositions and lead source of the Bainiuchang polymetallic deposit, southeast Yunnan. China. Geochem. 42 (2), 116–130 (in Chinese with English abstract).
Li, K.W., Zhang, Q., Wang, D.P., Cai, Y., Liu, Y.P., 2013d. LA-MC-ICP-MS U-Pb geochronology of cassiterite from the Bainiuchang polymetallic deposit, Yunnan province. China. Acta Mineral. Sin. 33 (2), 203–209 (in Chinese with English abstract).
Liu, Y.B., Mo, X.X., Zhang, D., Que, C.Y., Di, Y.J., Pu, X.M., Cheng, G.S., Ma, H.H., 2014. Petrogenesis of the Late Cretaceous granite discovered in the Laojunshan region, southeastern Yunnan province. Acta Petrol. Sin. 30 (11), 3271–3286 (in Chinese with English abstract).
Liu, Y.P., Ye, L., Li, C.Y., Song, B., Li, T.S., Guo, L.G., Pi, D.H., 2006. Discovery of the Neoproterozoic magmatics in southeastern Yunnan: evidence from zircon U-Pb dating and lithogeochemistry. Acta Petrol. Sin. 22 (4), 916–926 (in Chinese with English abstract).
Liu, Y.P., Li, Z.X., Li, H.M., Guo, L.G., Xu, W., Ye, L., Li, C.Y., Pi, D.H., 2007. U-Pb geochronology of cassiterite and zircon from the Dulong Sn–Zn deposit: evidence for Cretaceous large-scale granitic magmatism and mineralization events in southeastern Yunnan province. China. Acta Petrol. Sin. 23 (5), 967–976 (in Chinese with English abstract).
Liu, Y.P., Li, Z.X., Ye, L., Tan, H,Q., Li, C.Y., 2011. Chronological study of tungsten deposit in Laojunshan. Acta Mineral. Sin. Sup., 617–618 (in Chinese with English abstract).
Ludwig, K.R., 2003. Isoplot v.3.0: a geological toolkit for Microsoft excel. Berkeley Geochronology Center, Special Publication No. 40, pp. 1–70.
Mahood, G., Hildreth, W., 1983. Large partition coefficients for trace elements in high silica rhyolites. Geochim. Cosmochim. Acta 47 (1), 11–30.
Maluski, H., Lepvrier, C., Jolivet, L., Carter, A., Roques, R., Beyssac, O., Tang, T.T., Thang, D.N., Avigad, D., 2001. Ar–Ar and fission-track ages in the Song Chay massif: Early Triassic and Cenozoic tectonics in northern Vietnam. J. Asian Earth Sci. 19 (1–2), 233–248.
Mao, J.W., Hua, R.M., Li, X.B., 1999. A preliminary study of large scale metallogenesis and large clusters of mineral deposits. Miner. Deposits 18 (4), 291–299 (in Chinese with English abstract).
Mao, J.W., Xie, G.Q., Guo, C.L., Chen, Y.C., 2007. Large-scale tungsten–tin mineralization in the Nanling region South China: metallogenic ages and corresponding geodynamic processes. Acta Petrol. Sin. 23 (10), 2329–2338 (in Chinese with English abstract).
Mao, J.W., Xie, G.Q., Guo, C.L., Yuan, S.D., Cheng, Y.B., Chen, Y.C., 2008. Spatial-temporal distribution of Mesozoic ore deposits in South China and their metallogenic settings. Geol. J. China Univ. 14 (4), 510–526 (in Chinese with English abstract).
Mao, J.W., Cheng, Y.B., Chen, M.H., Pirajno, F., 2013. Major types and time-space distribution of Mesozoic ore deposits in South China and their geodynamic settings. Mineral. Deposita 48 (3), 267–294.
Middlemost, E.A.K., 1994. Naming materials in the magma/igneous rock system. Earth Sci. Rev. 37 (3–4), 215–224.
Mo, X.X., Zhao, Z.D., Deng, J.F., Dong, G.C., Zhou, S., Guo, T.Y., Zhang, S.Q., Wang, L.L., 2003. Response of volcanism to the India-Asia collision. Earth Sci. Front. 10 (3), 135–148 (in Chinese with English abstract).
Müller, A., Thomas, R., Wiedenbeck, M., Seltmann, R., Breiter, K., 2006. Water content of granitic melts from Cornwall and Erzgebirge: A Raman spectroscopy study of melt inclusions. Eur. J. Mineral. 18 (4), 429–440.
Niu, Y.L., 2005. Generation and evolution of basaltic magmas: some basic concepts and a new view on the origin of Mesozoic-Cenozoic basaltic volcanism in Eastern China. Geol. J. China Univ. 11 (1), 9–46 (in Chinese with English abstract).
Pan, J.B., Zhang, D., Que, C.Y., Di, Y.J., Huang, K.W., Bi, M.F., Xu, J.Z., 2015. Geochemistry and zircon U-Pb chronology of the Laochengpo gneissic granite in the southeast Yunnan area and their implications. Bull. Mineral. Petrol. Geochem. 34 (4), 795–803 (in Chinese with English abstract).
Qi, L., Hu, J., Gregoire, D.C., 2000. Determinition of trace elements in granites by inductively coupled plasma mass spectrometry. Talanta 51 (3), 507–513.
Qin, D.X., Li, Y.S., Tan, S.C., Chen, A.B., Xue, C.D., Fan, Z.G., Dang, Y.T., Tong, X., Wu, J.D., Li, Y.X., Wang, H.Y., 2006. Metallogenic ages of Gejiu tin ore deposit in Yunnan province. Chinese J. Geol. 41 (1), 122–132 (in Chinese with English abstract).
Roger, F., Leloup, P.H., Jolivet, M., Lacassin, R., Trinh, P.T., Brunel, M., Seward, D., 2000. Long and complex thermal history of the Song Chay metamorphic dome (Northern Vietnam) by multi-system geochronology. Tectonophysics 321 (4), 449–466.
Rollinson, H.R., 1993. Using geochemical data: evaluation, presentation, interpretation. Longman, Essex, England, pp. 1–352.
Rudnick, R.L., Gao, S., 2003. The composition of the continental crust. A2 - Holland, Heinrich D. In: Turekian, K.K. (Ed.), Treatise on Geochemistry. Pergamon, Oxford, pp. 1–64.
Sun, S., McDonough, W.F., 1989. Chemical and isotopic systematics of oceanic basalts, implications for mantle composition and processes. Geological Society, London, Special Publications 42, 313–345.
Sun, W.D., Ding, X., Hu, Y.H., Li, X.H., 2007. The golden transformation of the Cretaceous plate subduction in the west Pacific. Earth Planet. Sci. Lett. 262 (3–4), 533–542.
Sun, W.D., Zhang, H., Ling, M.X., Ding, X., Chung, S.L., Zhou, J.B., Yang, X.Y., Fan, W.M., 2011. The genetic association of adakites and Cu–Au ore deposits. Int. Geol. Rev. 53 (5–6), 691–703.
Sylvester, P.L., 1998. Post-collisional strongly peraluminous granites. Lithos 45 (1–4), 29–44.
Tan, H.Q., Liu, Y.P., 2017. Metamorphism and deformation of the Mengdong Group-Complex in southeastern Yunnan province and their tectonic implications. Acta Geol. Sin. 91 (1), 15–42 (in Chinese with English abstract).
Thomas, R., Förster, H.J., Rickers, K., Webster, J.D., 2004. Formation of extremely F-rich hydrous melt fractions and hydrothermal fluids during differentiation of highly evolved tin-granite magmas: a melt/fluid-inclusion study. Contrib. Mineral. Petrol. 148 (5), 582–601.
Tu, G.C., 2002. Two unique mineralization areas in Southwest China. Bull. Mineral. Petrol. Geochem. 21 (1), 1–2 (in Chinese with English abstract).
Vervoort, J.D., Patchelt, P.J., Gehrels, G.E., Nutman, A.P., 1996. Constraints on early earth differentiation from hafnium and neodymium isotopes. Nature 379, 624–627.
Wang, C.S., Li, X.H., Hu, X.M., 2003. Age of initial collision of India with Asia: review and constraints from sediments in Southern Tibet. Acta Geol. Sin. 77 (1), 16–24 (in Chinese with English abstract).
Wang, C.Y., Han, R.S., Huang, J.G., Xu, S.H., Ren, T., 2019. The ^{40}Ar–^{39}Ar dating of biotite in ore veins and zircon U-Pb dating of porphyrtic granite dyke in the Nanyangtian tungsten deposit in SE Yunnan. China. Ore Geo. Rev. 114, 103133.
Wang, Q., Li, J.W., Jian, P., Zhao, Z.H., Xiong, X.L., Bao, Z.W., Xu, J.F., Li, C.F., Ma, J.L., 2005. Alkaline syenites in eastern Cathaysia (south China): link to Permian-Triassic transtension. Earth Planet. Sci. Lett. 230 (3–4), 339–354.
Wang, X.J., Liu, Y.P., Miao, Y.L., Bao, T., Ye, L., Zhang, Q., 2014. In-situ LA-MC-ICP-MS cassiterite U-Pb dating of Dulong Sn–Zn polymetallic deposit and its significance. Acta Petrol. Sin. 30 (3), 867–876 (in Chinese with English abstract).
Watson, E.B., Harrison, T.M., 1983. Zircon saturation revisited: temperature and compositional effects in variety of crustal magma types. Earth Planet. Sci. Lett. 64 (2), 295–304.
Werner, T.T., Mudd, G.M., Jowitt, S.M., 2017. The world's by-product and critical metal resources part iii: a global assessment of indium. Ore Geol. Rev. 86, 939–956.
Whalen, J.B., Currie, K.L., Chappell, B.W., 1987. A-type granites: geochemical characteristics, discrimination and petrogenesis. Contrib. Mineral. Petrol. 95 (4), 407–419.
Wu, G.Y., Ji, J.Q., He, S.D., Zhong, D.L., 2002. Early Permian magmatic arc in Pingxiang, Guangxi and its tectonic implications. J. Mineral. Petrol. 22 (3), 61–65 (in Chinese with English abstract).
Xia, Y., Liu, L., Xu, X.S., 2016. Late Mesozoic A-type granitoids in SE China and Paleo-Pacific plate subduction and slab rollback. Bull. Mineral. Petrol. Geochem. 35 (6), 1109–1119 (in Chinese with English abstract).
Xu, B., Jiang, S.Y., Wang, R., Ma, L., Zhao, K.D., Yan, X., 2015. Late cretaceous granites from the giant dulong sn-polymetallic ore district in yunnan province, south china: geochronology, geochemistry, mineral chemistry and Nd–Hf isotopic compositions. Lithos 218–219, 54–72.
Xu, X.S., Xie, X., 2005. Late Mesozoic-Cenozoic basaltic rocks and crust-mantle interaction. SE China. Geol. J. China Univ. 11 (3), 318–334 (in Chinese with English abstract).
Yan, D.P., Zhou, M.F., Wang, Y., Wang, C.L., Zhao, T.P., 2005. Structural styles and chronological evidences from Dulong Song Chay tectonic dome: earlier spreading of South China Sea Basin due to Late Mesozoic to Early Cenozoic extension of South China Block. Earth Sci.-J. China Univ. Geosci. 30 (4), 402–412 (in Chinese with English abstract).
Yang, Z.X., Mao, J.W., Chen, M.H., Tong, X., Wu, J.D., Cheng, Y.B., Zhao, H.J., 2008. Re–Os daitng of molybdenite from the Kafang skarn copper (tin) deposit in the Gejiu tin polymetallic ore district and its geological significance. Acta Petrol. Sin. 24 (8), 1937–1944 (in Chinese with English abstract).
Ye, L., Bao, T., Liu, Y.P., Zhang, Q., Wang, X.J., He, F., Wang, D.P., Lan, J.B., 2016. Mineralization stages and ore-forming fluid of Dulong Sn–Zn polymetallic ore deposit, Yunnan Province. China. Acta Minerl. Sin. 36 (4), 503–509 (in Chinese with English abstract).
Yokart, B., Barr, S.M., Williams-Jones, A.E., Macdonald, A.S., 2003. Late-stage alteration and tin-tungsten mineralization in the Khuntan Batholith, northern Thailand. J. Asian Earth Sci. 21 (9), 999–1018.
Yuan, H.L., Gao, S., Dai, M.N., Zong, C.L., Günther, D., Fontaine, G.H., Liu, X.M., Diwu, C.Y., 2008. Simultaneous determinations of U-Pb age, Hf isotopes and trace element compositions of zircon by excimer laser-ablation quadrupole and multiple-collector ICP-MS. Chem. Geol. 247 (1), 100–118.
Yurimoto, H., Duke, E.F., Papike, J.J., Shearer, C.K., 1990. Are discontinuous chondrite-normalized REE patterns in pegmatitic granite systems the results of monazite fractionation? Geochim. Cosmochim. Acta 54 (7), 2141–2145.
Zeng, Z.G., Li, C.Y., Liu, Y.P., Tu, G.C., 1998. Ree geochemistry of scheelite of two genetic types from Nanyangtian, southeastern Yunnan. Geol. Geochem. 26 (2), 34–38 (in Chinese with English abstract).
Zhang, B.Y., Zhang, H.X., Zhao, Z.H., Yang, S.F., Chen, H.L., Shi, M.Q., 2003a. Permian island- arc basalt in West Guangdong and East Guangxi tectonic belt, South China: implications for the Paleotethys. J. Nanjing Univ. 39 (1), 46–54 (in Chinese with English abstract).
Zhang, K.J., Cai, J.X., Zhu, J.X., 2006. North China and South China collision: insights from analogue modeling. J. Geodyn. 42 (1–3), 38–51.
Zhang, Q., Liu, Z.H., Zhan, X.Z., Shao, S.X., 2003b. Specialization of ore deposit types and minerals for enrichment of indium. Miner. Deposits 22 (1), 309–316 (in Chinese with English abstract).
Zhang, S.T., 2011. Late Yanshanian acid magmatic activity and metallogenesis in Southeast Yunnan. Academic Salon (in Chinese).
Zhang, Y., Huang, Z.L., Luo, T.Y., Qian, Z.K., Zhang, J.W., Sun, J.B., 2013. The geochemistry and SIMS U-Pb zircon dating of the Jiasha gabbric-monzonitic intrusion in Gejiu district. Yunnan Province. Geochim. 42 (6), 523–543 (in Chinese with English

abstract).
Zhang, Y.Q., Xu, X.B., Jia, D., Shu, L.S., 2009. Deformation record of the change from indosinian collision-related tectonic system to Yanshanian subduction-related tectonic system in South China during the Early Mesozoic. Earth Sci. Front. 16 (1), 234–247 (in Chinese with English abstract).
Zhang, Y.H., Zhang, S.T., Tan, S.C., Cui, Y.L., Zhao, Z.F., Jiang, Y.G., Jiang, S.D., Tao, S.Y., 2016. The genetic relationship between the large Guanfang W deposit and granitic intrusions, in Yunnan Province, southwest China: evidence from U-Pb and Re–Os geochronology and Pb and Sr isotopic characteristics. Ore Geol. Rev. 79, 332–345.
Zhao, Y.G., Zhong, D.L., Liu, J.H., Wu, H., Liu, F.T., 1992. Fundamentals of geological interpretation for seismic tomography and its application to studying of west Yunnan's deep structure. Chinese J. Geol. 4 (2), 105–113 (in Chinese with English abstract).
Zhong, D.L., Wu, G.Y., Ji, J.Q., Zhang, Q., Ding, L., 1998. The ophiolite found in southeastern Yunnan. Chinese Sci. Bull. 43 (13), 1365–1369.
Zhou, X.M., Li, W.X., 2000. Origin of Late Mesozoic igneous rocks of southeastern China: implications for lithosphere subduction and underplating of mafic magma. Tectonophsics 326 (3), 269–287.
Zhou, X.M., Sun, T., Shen, W.Z., Shu, L.S., Niu, Y.L., 2006. Petrogenesis of Mesozoic granitoids and volcanic rocks in South China: a response to tectonic evolution. Episodes 29 (1), 26–33.